Document: WSRC-RP-92-582

Title: "Characterization of the Airborne Activity Confinement System Prefilter Material (U)"

WSRC-RP--92-582

DE93 004260

APPROVALS

Ted A. Long — 7/28/92
Author, T.A. Long — Date

Paul R. Monson — 7/24/92
Author, P.R. Monson — Date

R Graves — 7/25/92
Technical Reviewer, R. Graves — Date

J. C Britt — 7/27/92
Severe Accident Lead Engineer, T.E. Britt — Date

L.A. Wooten — 8/10/92
Safety Analysis and Engineering Services Manager, L.A. Wooten — Date

M J Hitchler — 8/21/92
Safety Technology Section Manager, M. Hitchler — Date

TABLE OF CONTENTS

INTRODUCTION

A general concern with assessing the effects of postulated severe accidents is predicting and preventing the release of radioactive isotopes to the environment at the Savannah River Site (SRS) reactor. Unless the confinement systems are breached in an accident the Airborne Activity Confinement System forces all of the internal air through the filter compartments. Proper modeling of the radioactivity released to the environment requires knowledge of the filtering characteristics of the demisters, the HEPA's, and the charcoal beds.

An investigation of the mass loading characteristics for a range of particle sizes was performed under the direction of Vince Novick of Argonne National Laboratory (ANL) for the Savannah River Technology Center (SRTC) in connection with the restart of the K reactor. Both solid and liquid aerosols were used to challenge sample prefilter and HEPA filters. The results of the ANL investigation were reported in a document titled "Characterization of the Airborne Activity Confinement System Prefilter Material (U)". The document is included here as Appendix I and is reviewed and interpreted with regard to MELCOR/SR and the SRS reactors.

RESULTS

Prefilter efficiency

Experiments were conducted at two velocities and with either solid and liquid aerosols. The two velocities, 152 cm/s and 53 cm/s, roughly correspond to the maximum and minimum expected operational velocities of the prefilters in the AACS.

The test results for the solid particle challenge aerosol at both test velocities are given in Table III of the paper in Appendix I. For particles with a Mass Median Aerodynamic Diameter (MMAD) greater than 4 μm the prefilter efficiency was between 90 and 100%. The prefilter efficiency decreased slightly to 80 to 90% for particles with MMAD between 1.43 and 2.5 μm. For particles smaller than 1.0 μm the efficiencies continue decreasing until, for all particles smaller than 0.1 μm, the efficiency drops to 0%. A least square fit of a line to the data resulted in a 50% efficiency for 0.69 μm MMAD solid particles. At the lower velocity the efficiency decreased for a given MMAD with the 50% efficiency MMAD equal to 1.02 μm. The reason for the decrease in efficiency at lower velocity is that the primary collection mechanism for the prefilter is inertial impaction. Lower velocities give the particles more time to respond to changes in the streamlines as they pass by the fibers.

The test results for challenge aerosols which consisted solely of liquid particles are presented in Table IV of Appendix I. At a given velocity, the efficiency as a function of MMAD was essentially the same as for the solid particle aerosol.

Mass loading tests

The mass loading tests were conducted at the 152 cm/s velocity and included both a prefilter and a HEPA filter. The filters were subjected to both liquid particle and solid particle aerosols and to a combined liquid/solid aerosol.

The liquid mass loading data results for the prefilter are presented in Table V of the paper in Appendix I. Liquid mass loading did not change the efficiency of the filter for any of the tested particle sizes. The pressure drop due to liquid mass loading was essentially zero for all tested particle sizes. Some scatter is visible in the data due to the resolution of the pressure transducer.

The mass loading on the HEPA filter depends on the efficiency of the prefilter. For the larger particles (MMAD = 3 μm), the prefilter efficiency was very high and little or no aerosol reached the HEPA filter. As the prefilter

efficiency decreased with decreasing particle size, the amount of aerosol penetrating the prefilter and challenging the HEPA filter increased. Unlike the prefilter, the pressure drop across the HEPA filter increased with mass loading and was a function of particle size.

Consistent with the simplified Bergman model of section 3.3 in the paper of Appendix I, the pressure drop across both the prefilter and the HEPA filter increased linearly with the mass loading for solid particles. For a given mass loading with solid particles, the pressure drop increased as the particle size decreased and, when the pressure data were scaled by the particle size the data collapsed onto a single line. In addition, the specific resistance of the prefilter was inversely proportional to the particle diameter. As in previous work (Novick, et. al., 1989, 1990a,b) the pressure drop across the HEPA filter varied linearly with the mass loading. The dependence of the pressure drop across the HEPA filter on particle size was unclear from experiments discussed in Appendix I since the aerosol distribution was not measured between the prefilter and the HEPA filter. Information on the HEPA filter performance is available in Novick and Higgins (1989).

Since an accident may release both liquid and solid aerosols, tests were run with a mixed aerosol. Both the solid and the liquid particles had approximately 2 μm MMAD. The pressure drop across the prefilter for a given mass loading of mixed particles exceeded the pressure drop for all solid particle sizes tested. Thus, while the pressure drop for liquid particles ($\Delta P = 0$) provides a minimum, the pressure drop for the solid particles does not provide a maximum bound for mixed aerosols.

CONCLUSIONS

General

Based on efficiency tests of the prefilter material, large particles (MMAD > 4 μm) are 100% filtered. The efficiency drops monotonically with particle size until MMAD = 0.1 μm below which no filtering occurs. The efficiency results are similar for solid and liquid particles.

For liquid aerosols, the pressure difference across the prefilter due to mass loading is equal to zero for all particle sizes tested. The lack of a pressure increase with mass loading indicates that the liquid film which forms on the filter fibers is small enough that it has a negligible effect on the filter resistance. At high mass loadings, liquid drops were re-entrained into the air flow on the downstream side of the prefilter. The re-entrained droplets were relatively large and did not remain suspended long enough to challenge the HEPA filter downstream of the prefilter. Excess liquid on the prefilter fibers drained out the bottom of the filter as well. When the liquid particles challenge the HEPA directly, i.e. without prefiltering, the pressure drop across the HEPA due to liquid aerosol is a linear function of mass loading and also depends on the particle size.

For solid particles, both the prefilter and HEPA filter pressure drops are linear functions of mass loading for a given particle size. As particle size decreases, the pressure drop corresponding to a particular mass loading increases.

Tests using a mixed solid/liquid aerosol to challenge the prefilter show that the solid particle pressure drops do not bound the mixed particle pressure drops.

Application to the AACS

A semi-empirical theory for pressure drop and mass loading due to solid particles is presented in section 3.3 of the paper in Appendix I. Given experimentally determined values for the specific resistance of the particle cakes on the prefilter and the HEPA and the filter efficiencies, a target pressure drop across the two filters, and a particle size, the mass loading across the AACS can be estimated by solving a system of four equations with four unknowns. For the specific case of ΔP_{AACS} = 1750 Pa, V = 1.8 m/s, and all five filter compartments operational, the theoretical prediction is within 25% of the extrapolated experimental results.

The theory for liquid particles is not well developed and the simplified model for mass loading of liquid particles is essentially an extrapolation of experimental data. Specific resistances can not be calculated for liquid particles since a particle cake does not develop. Taking ΔP_{AACS} = 1750 Pa, $\Delta P_{prefilter}$ = 0 Pa, and estimating the mass on the HEPA from the experimental data, the mass loading for various particle sizes was calculated.

Implications for MELCOR/SR

The current version of MELCOR/SR treats the AACS filters as a group of flow paths. Each of the five filter compartments is modeled as three sequential flow paths, one each for the demister, the HEPA filter, and the charcoal beds. The charcoal beds collect the iodine vapors which are not filtered by either the prefilter or the HEPA filter and thus are not important to AACS aerosol loading.

The current input deck used in MELCOR/SR-MOD3 deposits only the water droplets on the demisters, with an efficiency of 99.7%. The remaining aerosols (both solid and liquid) and the 0.3% of the water droplets which pass through the prefilter which have diameters greater than 0.025 μm are filtered with 99.7% efficiency by the HEPA filters. The pressure drop across the prefilter due to mass loading was assumed to be zero which, based on the paper in Appendix I, is valid so long as only liquid aerosols are retained. The pressure drop across the HEPA due to mass loading was assumed to be a linear function of the mass on the filter. The input deck uses a slope of 25.1 Pa/kg for the mass loading line, which is based on Novick and Higgins (1989) predicted mass loading characteristics for one 32-unit SRS HEPA filter bank loaded with 1.30 μm MMD (mass median diameter) solid particles.

Both the demister and HEPA filter models can be improved by considering the work in Appendix I. In reality, the aerosol challenging the prefilter consists of both solid and liquid particles of varying size. The demister collects all of the particles larger than 4 μm MMD, none of the particles less than 0.1 μm MMD, and some fraction of the particles in between those two limits. The addition of solid particles to the prefilter material would change the ΔP = 0 assumption for the prefilter mass loading. Thus, the MELCOR/SR filter model underpredicts the pressure drop across the prefilter due to mass loading. The demister model in MELCOR/SR can easily be modified to allow for capture of large solid and liquid aerosol particles in addition to water droplets. The addition of large solid aerosols to the prefilter would require a linear expression for the pressure drop as a function of mass loading (available from Appendix I over a range of particle sizes) as for the current HEPA filter model. The demister mass loading characteristics are also functions of particle size.

The dependence of the pressure drop on particle size can be simplified by approximating the product of the pressure drop and the particle diameter as a linear function of the mass loading. (See figure 3-7 in Appendix I.)

The filter cutoff point for the prefilter is not modelled correctly. The current assumption of a step function between 99.7% and 0% efficiency is a convenient simplification and may be acceptable if the cutoff point is chosen appropriately. The current cutoff point for the prefilter is zero, so that all particle diameters (recall that the prefilter only operates on water droplets in the current model, though) are filtered. The experiments in Appendix I, however, show that 100% of particles smaller than 0.1 μm in diameter penetrate the prefilter material. Thus, the prefilter model retains more water droplets than it should but does not account for any of the additional solid and liquid aerosols which would be expected to be captured. The predicted total pressure drop across the prefilter due to mass loading is too small. The associated mass loading on the prefilter could be too high since the MELCOR/SR filter model captures particles which are considerably smaller than the experimentally determined cut off diameter in Appendix I. The predicted mass loading on the prefilter, however, is almost certainly too low since the MELCOR/SR filter model does not account for the liquid aerosol particles other than water nor for the large solid aerosol particles which are captured by the prefilter.

As mentioned above, the current HEPA filter model in MELCOR/SR uses a pressure drop that is a linear function of mass loading. The actual coefficients are based on data from Novick and Higgins (1989) for a specific solid particle size. While the HEPA filter model does use a linear pressure drop, the effect of particle size on the pressure drop is not taken into account. Particle size distribution information is available from MELCOR/SR and could be included in the model through additional control functions. In addition, the HEPA filter will likely be challenged by both solid and liquid particles which, according to the paper in Appendix I, increases the pressure drop associated with a given mass loading. Thus, the HEPA filter model includes linear increases in pressure drop with mass loading but in an incomplete fashion since particle size and mixed aerosol effects are not included. If the particle size from which the HEPA filter model pressure drop is taken represents an average particle size of the challenge aerosol then the pressure drop of solid aerosol loading will still be approximately correct. However, the pressure drop across the HEPA filter is likely to be underpredicted since mass loading by mixed liquid/solid aerosols increases the pressure drop for a given mass loading.

The cutoff point for the HEPA is currently .025 μm. HEPA filters, however, do not have minimum collection diameters. The filter fibers are so

dense that small particles are collected at 100% efficiency due to diffusion effects. Large particles are collected at 100% efficiency due to impaction and interception effects. At some point between large and small particles is a minimum efficiency, which for the MELCOR/SR model of the SRS HEPA filter material is 99.97%. Thus, the cutoff point should be set to zero for the HEPA filters.

MELCOR/SR runs to date have predicted that filter failure is not a concern. The predictions, however, were based on a filter model which underpredicts the pressure drop across both the prefilter and the HEPA filter and does not account for mass loading on the pre-filter. The current filter models are conservative from the standpoint of allowing more particles through the AACS than expected, thus increasing the release to the environment during normal filter operation. Since the demister only collects water droplets, the HEPA filter model is challenged by more mass than the actual HEPA filters. While the mass loading on the HEPA's may be overpredicted, the pressure drop and margin to failure could be underpredicted since the higher pressure drops associated with mixed solid/liquid aerosol loading are not accounted for. The current filter models predict so little mass loading that filter failure may not be a concern but MELCOR/SR sensitivity studies should be made with more accurate, or at least conservative from the standpoint of potential filter failure, filter models. These study results should be reviewed and applied in all future SRS analyses using MELCOR/SR.

REFERENCES

Bergman, W., Taylor, R.D., Miller, H.H., Biermann, A. H., Hebard, H.D., da Roza, R.A., Lum, B.Y. (1978), "Enhanced filtration program at LLNL. A Progress Report." 15th DOE Nuclear Air Cleaning Conference, CONF-780819, Boston.

Billings, C.E., Handbook of Fabric Filter Technology, Volume 1, PB-200648, NTIS, December 1970, pp. 137-8.

Novick, V.J., Abrahamson, C.A., and Richardson, W.B. (1990a), "Relationship Between the Pressure Drop Across the Savannah River Site's HEPA Filter Material and Aerosol Mass Loading," WSRC-RP-90-779.

Novick, V.J., Higgins, P.J. (1989) "Phase 1 Characterization of the HEPA Filter Media used in the Airborne Activity Confinement System at the Savannah River Site," WSRC-RP-89-793.

Novick, V.J., Higgins, P.J., Dierkeshiede, B., Abrahamson, C., and Richardson, W.B. (1990b), "Efficiency and Mass Loading Characteristics of a Typical HEPA Filter Media Material," 21st DOE Nuclear Air Cleaning Conference.

APPENDIX I

CHARACTERIZATION OF THE AIRBORNE ACTIVITY CONFINEMENT SYSTEM PREFILTER MATERIAL

by

Vincent J. Novick
Jane F. Klassen
Jeffrey J. Sciortino

Engineering Physics Division
Argonne National Laboratory
Argonne, IL 60439

AUGUST 1991

Under Contract to the Westinghouse Savannah River Company

Abstract

Particle removal efficiencies of the prefilter material under conditions simulating the those found in the Savannah River Site's Airborne Activity Confinement System (AACS) were measured as a function of particle size, media velocity of the aerosol, and the composition of the aerosol (liquid or solid). Based on a least square fit to the data for both solid and liquid aerosols, the diameter that is collected with a 50% efficiency, d_{50}, is 0.60 μm for gas flow velocities of 152 cm/s and 0.87 μm for gas velocities of 53 cm/s. These velocities correspond to AACS volumetric flows of 100,000 cfm and 33,000 cfm, respectively.

The mass loading characteristics of the prefilter material at the expected nominal velocity conditions in the AACS were measured as a function of the pressure difference across the prefilter, particle size, and composition of the aerosol (liquid, solid, or mixed). Results indicate that, for liquid aerosols the pressure drop remains constant as a function of mass loading in the prefilter material and can be approximated by the initial clean pressure drop across the prefilter. For solid particles, the increase in the pressure difference across the prefilter as a function of mass loading was measured for three different particle size distributions of aluminum oxide. The change in the specific resistance of the prefilter cake was plotted as a function of particle diameter.

The efficiency curve fit to the experimental data and the correlation for the specific resistance were used to predict the mass loading characteristics of the AACS, specifically the prefilter and the High Efficiency Particulate Air (HEPA) filter elements of the system, as a function of particle size for a given pressure difference. These predictions from the generalized correlation equations were compared to specific extrapolations of the AACS loading based on the

actual experimental mass loadings and the ratio of the areas between the experimental filters and the AACS filters. The predictions agreed with the extrapolated experimental values to within 25%. This agreement indicates the level of usefulness of the predictive equations developed in this work.

CONTENTS

LIST OF FIGURES

Nomenclature

A	=	surface area of the filter
A_1	=	Liew and Condor correlation coefficient
C	=	slip correction factor
D	=	diffusion coefficient
D_P	=	particle size distribution challenging the AACS prefilter
D_H	=	particle size distribution challenging the AACS HEPA filter
d_{50}	=	particle diameter at which the filter is 50% efficient
d_f	=	fiber diameter
d_p	=	diameter of particle
E	=	efficiency
f	=	fraction of gas swept by filter
h	=	depth of filter material
k	=	Boltzmann constant
K_2	=	specific resistance of the cake
Ku	=	Kuwabara hydrodynamic factor
M	=	mass collected on filter
ΔP	=	total pressure difference
ΔP_c	=	pressure difference due to particle cake on filter
ΔP_f	=	final pressure difference across filter following test
ΔP_o	=	pressure difference across clean filter
ΔP_w	=	pressure difference across the wet filter
ΔP_{we}	=	pressure difference across the wet filter in an equilibrium condition
Q	=	volumetric flow rate
Re	=	Reynolds number
S_c	=	Schmidt number
t	=	surface tension of the liquid
T	=	temperature
V	=	velocity
α_f	=	filter solidity, or packing (volume) density
α_p	=	volume density of the particles
η	=	efficiency
η_i	=	efficiency due to impaction
η_d	=	efficiency due to diffusion
η_I	=	efficiency due to interception
μ	=	gas viscosity
ρ	=	density of particle
ϕ	=	contact angle of a droplet with respect to the fiber's surface
Ψ	=	Stokes number

1.0 INTRODUCTION

The purpose of this work is to answer some of the questions posed by the general problem of predicting and preventing release of radioactive isotopes from Savannah River reactors to the environment. It is generally recognized that, for severe accidents, a significant fraction of this postulated release of radioactive isotopes will be in the form of aerosols. Specifically, this work addresses the ability of the Airborne Activity Confinement System (AACS) [Tinnes and Petry, 1986], [Petry et al, 1985] used in the production reactors at the Savannah River Site to provide for the capture and confinement of these accidentally released radioisotopes. Figure 1-1 shows a schematic diagram of the AACS. Outside air is continuously drawn through the building by fans and exhausted out the stack. The exhaust fans maintain the reactor room and other areas of the building at a negative pressure so that any material released inside the building cannot exit to the outside environment without passing through a series of filters.

The first filter in the filter compartment is the demister/prefilter also referred to as a moisture separator. In an accident scenario where steam is released, the steam in the reactor building will cool, condense and form a fog of water droplets. The demister/prefilter is designed primarily to remove water droplets but will also remove any other large aerosol particles before they can be deposited in the High Efficiency Particulate Air (HEPA) filter. These HEPA filters comprise the second filter in the filter compartment. The HEPA filter is designed to remove all particles from the gas stream with efficiencies of at least 99.97%. Previous tests [Novick et al, 1989] have measured the HEPA filter efficiency to be 99.9727% for 0.15 μm mass median aerodynamic diameters (MMAD) at an operating flow velocity of 2.98 cm/s. The HEPA filter efficiency was determined to be a minimum of 99.9886% for a

0.3 μm MMAD at the minimum operating flow velocity of 0.89 cm/s. The final component in the filter compartment is a carbon bed, which removes more than 99.9% of the elemental iodine vapors from the exhaust gas [Tinnes and Petry, 1986].

This work was performed at Argonne National Laboratory between April 1990 and August 1991 under the sponsorship of Westinghouse Savannah River Company. This report presents the results of the characterization of the demister/prefilter material used in the AACS. The first task was to measure the demister/prefilter collection efficiency. Monodisperse particles of various diameters were generated to challenge the prefilter. For certain size ranges, monodisperse particles could not be generated, therefore more polydisperse distributions were used. The efficiency of the prefilter material is determined by measuring the number or weight of particles collected on a scaled prefilter against the total number or weight of particles challenging the prefilter. Measurements were taken at two different air flow velocities; one corresponding to an AACS exhaust flow of 100,000 cfm (152 cm/s), representing the nominal operating flow conditions, and the other approximately 1/3 of the operating flow, or 33,000 cfm (53 cm/s). The lower tested flow rate is just below the minimum operational flow through the filter compartment of 40,000 cfm, required to maintain the minimum acceptable negative pressure in the building.

The second task was to measure the pressure drop across the demister as a function of particle mass loading. For this task a scaled prefilter was tested in series with a similarly scaled HEPA filter to determine the overall behavior of the AACS. The change in the pressure drop with mass loading was studied for three different size particle distributions corresponding to maximum collection, nominally 50% collection and maximum penetration through the prefilter. The pressure drop as a function of mass loading of the prefilter and HEPA filter was studied using both solid and liquid particles. The measurements were taken at air flow velocities of 152 cm/s through the prefilter and 3 cm/s through the HEPA filter.

The final section of this report uses the correlations for the prefilter efficiency and mass loading as a function of particle size, developed in the first two tasks, in conjunction with HEPA filter mass loading correlations developed in earlier work [Novick et al, 1990b] to provide a method of predicting the total mass loading on the AACS for a given particle diameter, density, filtration velocity and final ΔP across the AACS. Experimental data from the mass loading tests was extrapolated to determine the total mass that would be collected by the AACS for the three test conditions. These extrapolated values are compared with the predicted values to show the level of confidence in the prediction.

2.0 EFFICIENCY TESTS

2.1 Experimental Description

Figure 2-1 shows a schematic of the experimental system used for determining the efficiency of the prefilter as a function of particle diameter. This system was designed to simulate the prefilter component of the AACS. The gas velocity through the filter media and the actual filter material properties such as filter fiber diameter, filter depth and porosity were set equal to those found in the AACS. The filtration area and hence the total flow rate was scaled to maintain the proper media velocity.

Clean, dry air was supplied to an aerosol nebulizer to produce liquid droplets. Various nebulizing methods and solution concentrations were used to provide a range of particle sizes. The various types of solutions used in the experiments are discussed later in Section 2.2. The aerosol output was mixed with clean, dry air in the mixing chamber and exhausted out through the prefilter and HEPA filter by a blower.

2.2 Apparatus for Aerosol Generation

2.2.1 Solid Particles

To provide a monodisperse output of solid particles, two aerosol generators were used. A TSI Model 3075/3076 Constant Output Atomizer (COA) was used with a TSI Model 3071 Electrostatic Classifier (EC) to generate particles in the submicron size range, with mass median aerodynamic diameters (MMADs) less than 0.5 μm. The Constant Output Atomizer produces a polydisperse aerosol of liquid droplets by directing a high velocity air jet across the end of a tube supplying a liquid reservoir. The liquid solution of fluorescein or sodium chloride and water is drawn up the tube by pressure difference and atomized by the air jet. Solid particles are formed after the water has evaporated. To insure complete evaporation of the water, a diffusion dryer was inserted in the system immediately after the aerosol atomizer. The polydisperse aerosol output from the atomizer is used as input to the Electrostatic Classifier which is used to select the desired monodisperse challenge aerosol. The Classifier consists of a bipolar diffusion charger and an electrical mobility analyzer. Aerosol particles are introduced into the bipolar charger where they interact with the bipolar ions, resulting in particles with a specific charge distribution. A specific charge to mass ratio of particles can be chosen by varying the voltage setting on an axial rod. This technique was suitable for generating monodisperse test particles up to 0.5 μm in diameter.

To generate particle diameters in the range of 1.5 μm and larger, a TSI Model 3450 Vibrating Orifice Generator was used. The Vibrating Orifice Generator (VOG) produces a monodisperse aerosol of known particle size, based upon the instability and breakup of a cylindrical liquid jet. By applying a periodic disturbance of an appropriate frequency on the liquid jet of constant flow rate, the breakup process can be controlled to produce uniform droplets. The final monodisperse particle size can be varied by changing the flow rate of the

liquid jet, concentration of a non-volatile solute in a solution, and to some extent by varying the vibrational frequency of break-up. These uniform droplets are dispersed by mixing with dry air.

2.2.2 Liquid Particles

Various methods of aerosol generation were used to obtain the monodisperse liquid particles. For these tests the TSI model 3075/3076 Constant Output Atomizer and Electrostatic Classifier were used to generate particles smaller than 0.5 μm and the VOG was used to generate monodisperse liquid particles larger than 2.5 μm. To generate particles in the region between 0.5 μm and 2.5 μm, two polydisperse methods were employed. A TSI Model 3072 Evaporation/Condensation Aerosol Conditioner was used with a 3-jet Collison atomizer to generate particles in the 0.05 μm to 1.0 μm size range. The operating principle of the 3-jet Collison atomizer is similar to the Constant Output Atomizer. The difference is that the Collison has 3 spray jets exiting the tube instead of one. By varying the concentration of the solutions, ethylene glycol, diethylene glycol and dioctyl phthalate, the output particle diameter can be controlled. The Evaporation/Condensation Aerosol Conditioner was used to narrow the output size distribution of the aerosol for the Collison. The TSI Constant Output Atomizer was also used alone to generate particle size distributions with MMAD's from 1.0 μm to 1.5 μm. As before, the size of the particle is dependent on the concentration of the solution.

Particle diameter determinations were made prior to each test using various methods, depending on the type of aerosol generator being used. The output particle diameter from the Electrostatic Classifier was determined by calculating the aerosol flow rates through the classifier as well as the proper voltage setting of the collector rod, utilizing mean electrical particle mobility and its relationship to the diameter of the particle. Particle diameters were also calculated when using the Vibrating Orifice Generator, from the volumetric concentration of the solute in the aerosol solution, the volumetric fraction of impurities in the solvent, the

liquid flow rate and vibrational frequency. The calculated particle diameters were periodically checked with either a Laser Aerosol Spectrometer or cascade impactor to assure the proper operation of the aerosol generator. For all other methods of aerosol generation the actual particle size distributions were measured for each test using either a Laser Spectrometer (LAS 250x) or a cascade impactor.

2.3 Particle Collection Apparatus

The prefilter mat is formed from individual teflon fibers with nominal diameters of 0.02 mm. The individual fibers are bundled into strands with resulting diameters ranging between 0.78 mm and 1.3 mm. The strands are woven into a mesh-like structure with the addition of fine stainless steel wire. The prefilter mat contains 24 layers (12 double layers) of this material which is compressed to a thickness of two inches within a stainless steel frame. Many of the fibers have been broken from the strands and protrude at various angles from the strands.

For these tests, the prefilter material was cut to a 10.2 cm x 12.7 cm (4 in x 5 in) rectangle and the edges of each double thickness piece were heat-sealed with fiberglass reinforced tape. These small prefilters were stacked together in the metal holder, designed to hold the 12 double layers of material, with thin closed cell foam gaskets between each piece. The resulting thickness of the prefilter mat was maintained at two inches. This arrangement was designed to force the gas and particles to flow through the filter and not bypass the filter material by going around the edges, as well as allowing repeated handling of the prefilter without fraying the edges. A metal frame covered the edges of the prefilters in their metal holder, leaving a rectangular face area of 7.6 cm x 10.2 cm (3 in x 4 in). This area was chosen so that a volume flow rate of approximately 25 cfm could be used to keep the experimental system velocity equal to the nominal velocity through the AACS. The entire prefilter holder was

attached to the aerosol mixing chamber as shown in Figure 2-1. Particles escaping through the prefilter were collected -- a 20.4 cm x 25.4 cm (8 in x 10 in) HEPA filter positioned downstream of the prefilter.

In the AACS, each prefilter presents an available filtration area of 56.8 cm x 56.5 cm (22.375 in x 22.25 in). The flow is distributed through 5 sets of compartments, each with 20 prefilter assemblies, 32 HEPA filters and 32 carbon beds. The effective filtration area of the each prefilter assembly is :

$$\text{Effective prefilter area} = 56.8\ \text{cm} \times 56.5\ \text{cm} = 3210\ \text{cm}^2$$
$$(22.375\ \text{in} \times 22.25\ \text{in} = 497.8\ \text{in}^2 = 3.457\ \text{ft}^2)$$

The nominal total flow rate through the AACS is about 100,000 to 120,000 cfm [Tinnes and Petry, 1986]. The lower AACS flow would result in a flow rate of at least 1000 cfm through each prefilter assembly. Testing at this flow rate will result in a conservative estimate of the efficiency but underestimate the quantity of liquid that might be re-entrained at the back face of the prefilter. However, re-entrainment is not expected to be a critical factor in reducing the efficiency of the prefilter because any re-entrained droplets should be relatively large, hence, easily removed from the gas stream before reaching the HEPA filter.

The gas velocity through the prefilter in the AACS can be calculated by:

$$\frac{1000\ \text{cfm}}{3.457\ \text{ft}^2} \times \frac{30.5\ \text{cm}}{1\ \text{ft}} \times \frac{1\ \text{min}}{60\ \text{sec}} = 150\ \text{cm/sec}$$

(150 cm/sec ~ 295 ft/min)

A velocity of 150 cm/s through the test prefilter with an effective area of 77.4 cm^2 (12 in^2) defines the volumetric flow rate through the test assembly to be 24.6 cfm. For the efficiency tests a flow controller with a 25.0 cfm setting was chosen resulting in a prefilter media test velocity of:

$$\frac{25.0\ \text{cfm}}{0.0833\ \text{ft}^2} \times \frac{30.5\ \text{cm}}{1\ \text{ft}} \times \frac{1\ \text{min}}{60\ \text{sec}} = 152\ \text{cm/sec}$$

One-third of the test velocity is:

$$\frac{8.6\ \text{cfm}}{0.0833\ \text{ft}^2} \times \frac{30.5\ \text{cm}}{1\ \text{ft}} \times \frac{1\ \text{min}}{60\ \text{sec}} = 53\ \text{cm/sec}$$

Particle collection efficiencies for the prefilter were tested at these two flow velocities, corresponding to a typical AACS exhaust flow of 100,000 cfm and at 33,000 cfm which is slightly less than the specified minimum flow of 40,000 cfm.

2.4 Efficiency Analysis Techniques

The efficiency of the prefilter was determined using either the ratio of particle counts upstream and downstream of the prefilter or the equivalent mass collected by the prefilter compared to the total mass of challenge aerosol. Sodium chloride was chosen to generate the solid particles used in the particle counting method of analysis. Efficiencies determined by particle counting utilized two Condensation Nucleus Counters (CNC), one sampling in the upstream flow and the other sampling in the downstream flow of the prefilter. Particle count conformity between the two CNCs was checked prior to using this method of analysis. The maximum difference in measurements on particle concentration ranges from 0.0 particles/cm^3 to 2000 particles/cm^3 was 3.8% between the two CNCs.

For each efficiency test, the CNCs sampled HEPA-filtered air to establish background (typically less than 1 part/cm^3). The aerosol was turned on and particle counting commenced after the system stabilized. Upstream and downstream particle counts were taken simultaneously for one minute. Several readings were taken to assure reproducibility and averaged to improve statistical accuracy. The downstream particle count rate was divided by the upstream particle count rate to determine the percent penetration of particles through the prefilter. The efficiency ratio was determined by subtracting the percent penetration from

100%. This method was used only for the small particles because the concentration of larger particles produced by the VOG was too low (within 10 times background) for accurate results.

The efficiency analysis for larger particles produced by the VOG used fluorescein as the solid particle and as a tracer in the liquid particle tests. This allowed the efficiency to be determined by comparing the mass collected by the prefilter to the total mass collected on the prefilter and HEPA filters. For solid particle efficiency tests, fluorescein was mixed in a sodium hydroxide and water solution and atomized using the Vibrating Orifice Generator. For liquid particle efficiency tests, fluorescein was used as a tracer in solutions of ethylene glycol, diethylene glycol and dioctyl phthalate (DOP), and either water or alcohol in the aerosol generators as described earlier.

Following each efficiency test using mass analysis, the prefilter and HEPA filter were removed from their holders and rinsed in separate sodium hydroxide/purified water solutions. These rinse solutions were analyzed with the Model 111 Turner Fluorometer. The intensity of the light re-emitted by a sample exposed to a constant ultraviolet light source is directly proportional to the concentration of fluorescein in the solution. These fluorometric readings were multiplied by the amount of rinse solution to obtain an equivalent mass. At least three rinses of each filter were made until the fluorometric reading was less than 10 times the background. The rinse results from each filter were summed to give separate equivalent mass results for the prefilter and the HEPA filter. The efficiency is the ratio of the equivalent mass on the prefilter to the total equivalent mass on the prefilter plus the HEPA filter.

Tables I and II list the solid and liquid particle diameters, the flow media velocity, the type of generator used, the type of analysis, and the concentration of the solution for each efficiency test.

TABLE I

SOLID PARTICLES

PARTICLE DIAMETER (μm)	FLOW RATE (cm/sec)	AEROSOL GENERATOR	ANALYSIS METHOD	SOLUTION CONCENTRATION
6.80	53	VOG	FLUORO	0.46%*
6.80	152/53	VOG	FLUORO	0.083%*
6 80	152/53	VOG	FLUORO	0.46%*
6.80	152/53	VOG	FLUORO	0.46%*
4.90	152/53	VOG	FLUORO	0.144%*
4.90	53	VOG	FLUORO	0.144%*
4.80	152/53	VOG	FLUORO	0.144%*
2.48	152/53	VOG	FLUORO	0.018%*
2.40	152/53	VOG	FLUORO	0.019%*
1.43	152/53	VOG	FLUORO	0.018%*
1.43	152	VOG	FLUORO	0.009%*
0.52	152/53	COA/EC	FLUORO	1%*
0.52	53	COA/EC	FLUORO	1%*
0.52	152/53	COA/EC	PT COUNT	10%†
0.45	152/53	COA/EC	PT COUNT	10%†
0.30	152	COA/EC	PT COUNT	10%†
0.25	152	COA/EC	FLUORO	1%*
0.25	152/53	COA/EC	PT COUNT	10%†
0.25	152/53	COA/EC	PT COUNT	10%†
0.05	152/53	COA/EC	PT COUNT	10%†
0.01	152/53	COA/EC	PT COUNT	10%†

* Fluorescein in Sodium Hydroxide
† Sodium Chloride in water

VOG = TSI Vibrating Orifice Generator
COA/EC = TSI Constant Output Atomizer/Electrostatic Classifier
FLUORO = Fluorometric analysis
PT COUNT = Particle counting analysis

TABLE II
LIQUID PARTICLES

PARTICLE DIAMETER (μm)	FLOW RATE (cm/sec)	AEROSOL GENERATOR	ANALYSIS METHOD	SOLUTION CONCENTRATION
7.14	152/53	VOG	EQMASS	0.477 % EG
5.18	152	VOG	EQMASS	0.178 % EG
5.00	152/53	VOG	EQMASS	0.165 % EG
1.16	53	COLL/EV	EQMASS	50 % DOP
1.14	152	COA	EQMASS	100 % DOP
0.82	152	COLL/EV	EQMASS	50 % DOP
0.67	152	COLL/EV	EQMASS	50 % EG
0.64	152	COA	EQMASS	100 % DOP
0.56	53	COLL/EV	EQMASS	50 % DEG
0.53	152/53	COA/EC	EQMASS	10 % DEG
0.53	152/53	COA/EC	PT COUNT	10 % EG
0.47	53	COLL/EV	EQMASS	1 % DEG
0.27	152	COLL/EV	EQMASS	50 % DEG
0.25	152/53	COA/EC	PT COUNT	10 % EG
0.19	152	COLL/EV	EQMASS	1 % DEG
0.12	152/53	COA/EC	PT COUNT	10 % EG

EG = Ethylene Glycol in sodium hydroxide and fluorescein
DEG = Diethylene Glycol in sodium hydroxide and fluorescein
DOP = Dioctyl Phthalate in propanol and fluorescein

VOG = TSI Vibrating Orifice Generator
COLL/EV = Collison 3-jet nebulizer with Evaporation Condensation Conditioner
COA = TSI Constant Output Atomizer
COA/EC = TSI Constant Output Atomizer with Electrostatic Classifier

EQMASS = Equivalent mass analysis
PT COUNT = Particle counting analysis

2.5 Experimental Efficiency Results

Measured efficiencies for the solid particle tests are given in Table III. Fig. 2-2 plots these efficiencies as a function of the mass median aerodynamic diameter (MMAD) of the particle at the high filtration flow velocity of 152 cm/s. Particles greater than 4 μm in diameter had efficiencies between 90 and 100% decreasing to a range of 80 to 95% efficiency for particle diameters between 1.43 and 2.5 μm. Collection efficiencies at particle diameters less than 0.1 μm were negligible. A least squares, linear curve fit to the experimental data yields a 50% efficiency of 0.69 μm for the prefilter at 152 cm/s for the solid particles.

Figure 2-3 is a plot of the efficiency versus MMAD for the lower filtration velocity of 53 cm/s. Collection efficiencies of 100% at a particle diameter of 7 μm were measured. The efficiency decreased to 80% at particle diameters of 4.9 μm. As with the higher flow velocity, the collection efficiency of particle diameters less than 0.1 μm is negligible. The least squares, linear curve fit to the experimental data yields a 50% efficiency of 1.02 μm for the prefilter at 53 cm/s for solid particles.

In general the efficiencies for the solid particles at 152 cm/s are greater than that at 53 cm/s. This is expected since the prefilter's primary collection mechanism is inertial impaction. The scatter in the data is somewhat greater than desired, and is probably due to a number of factors. First, comparison tests between the mass method and the count method indicated that the mass method consistently had much higher collection efficiencies than the count method for the same particle size. Second, there is sometimes a significant difference in the efficiencies measured between tests run at identical conditions. These differences are interpreted as being the result of prefilter variations in either structure (porosity, number of individual fibers protruding from the strands, etc.) or the lack of reproducibility in sealing the edges of the prefilter. Finally, the figures include both monodisperse and polydisperse data

which, for simplicity, had to be compared on the basis of MMAD's. Obviously, two distributions could have the same MMAD but different standard deviations possibly resulting in some of the scatter in the measured efficiencies.

The liquid particle efficiency test data is given in Table IV. The measured efficiencies as a function of MMAD for the 152 cm/s tests are presented graphically in Figure 2-4. A collection efficiency of 100% was measured for liquid particle diameters greater than 4.9 μm. At 0.1 μm, the collection efficiency was less than 30%. The least squares, linear curve fit to the experimental data yields an efficiency of 50% for 0.53 μm liquid particles for the prefilter at 152 cm/s.

Figure 2-5 is a plot of the prefilter collection efficiency for liquid particles versus MMAD at a test velocity of 53 cm/s. Collection efficiencies for droplets greater than 5 μm were between 97 and 100%. Collection efficiencies for 0.1 μm diameter particles were less than 20%. The least squares linear curve fit to the experimental data yields an efficiency of 50% for 0.65 μm liquid particles for the prefilter at 53 cm/s.

Similar to the solid particle efficiencies, the liquid particle efficiencies showed an overall trend of higher efficiencies at the higher velocity. There is an increased scatter in the data which is probably due to the use of more polydisperse particles and comparison of data on the basis of MMAD's. This increase in data scatter may also explain the difference between the 50% efficiencies of the solid and liquid curve fits at a given velocity.

TABLE III: SOLID PARTICLE EFFICIENCIES

NOMINAL EXHAUST FLOW 152.5 cm/s			ONE-THIRD NOMINAL FLOW 53.5 cm/s		
PARTICLE DIAMETER (μm)	EFFICIENCY %	AEROSOL ATOMIZER	PARTICLE DIAMETER (μm)	EFFICIENCY %	AEROSOL ATOMIZER
6.80	100.0	VOG	6.80	100.0	VOG
6.80	93.0	VOG	6.80	96.0	VOG
6.80	95.0	VOG	6.80	98.0	VOG
4.90	97.0	VOG	4.90	75.0	VOG
4.80	89.0	VOG	4.90	80.0	VOG
2.48	86.0	VOG	4.80	82.0	VOG
2.40	95.0	VOG	2.48	50.0	VOG
1.43	92.0	VOG	2.40	91.0	VOG
1.43	87.0	VOG	1.43	88.0	VOG
0.53	64.9	COA/EC	0.53	10.2	COA/EC
0.53	20.8	COA/EC	0.53	62.0	COA/EC
0.45	6.0	COA/EC	0.53	13.9	COA/EC
0.25	10.3	COA/EC	0.45	3.8	COA/EC
0.25	3.7	COA/EC	0.30	12.7	COA/EC
0.25	18.3	COA/EC	0.25	1.4	COA/EC
0.05	0.8	COA/EC	0.25	14.6	COA/EC
0.01	0.0	COA/EC	0.05	0.0	COA/EC
			0.01	0.0	COA/EC

VOG: VIBRATING ORIFICE GENERATOR
COA/EC: TSI CONSTANT OUTPUT ATOMIZER/ELECTROSTATIC CLASSIFIER

TABLE IV: LIQUID PARTICLE EFFICIENCIES

NOMINAL EXHAUST FLOW 152.5 cm/s			ONE-THIRD NOMINAL FLOW 53.5 cm/s		
PARTICLE DIAMETER (μm)	PERCENT EFFICIENCY	AEROSOL ATOMIZER	PARTICLE DIAMETER (μm)	PERCENT EFFICIENCY	AEROSOL ATOMIZER
7.14	100.0	VOG	7.14	97.0	VOG
5.18	100.0	VOG	5.10	100.0	VOG
4.90	100.0	VOG	1.16	27.0	COLL/EV
1.14	30.0	COA	0.56	33.0	COLL/EV
0.82	46.0	COLL/EV	0.53	18.0	COA/EC
0.67	58.0	COLL/EV	0.53	47.0	COA/EC
0.64	70.0	COA	0.47	51.0	COLL/EV
0.53	15.0	COA/EC	0.25	17.0	COA/EC
0.53	51.0	COA/EC	0.12	13.0	COA/EC
0.27	36.0	COLL/EV			
0.25	13.0	COA/EC			
0.19	31.0	COLL/EV			
0.12	20.0	COA/EC			

VOG: VIBRATING ORIFICE GENERATOR
COLL/EV : COLLISON 3-JET NEBULIZER WITH EVAPORATION CONDENSATION CONDITIONER
COA/EC: TSI CONSTANT OUTPUT ATOMIZER WITH ELECTROSTATIC CLASSIFIER

For comparison purposes Figures 2-6 and 2-7 present an overlay of both the solid and liquid particle efficiency data at high and low flow velocities, respectively. The least squares, linear curve fit for the 152 cm/s velocity curve yields a 50% efficiency of 0.60 μm, while the 50% efficiency point for the 53 cm/s velocity is 0.87 μm. These 50% points lie about halfway between those of the individual solid and liquid curves and appear to reasonably fit all of the data. Therefore, these empirically derived curve fits from experimentally measured data should provide the most accurate estimate of the prefilter collection efficiency for a given particle diameter.

2.6 Theory

The total efficiency of a filter can be calculated by combining the individual theoretical efficiencies due to impaction, interception and diffusion. Theoretical expressions exist for each of these mechanisms, but usually semi-empirical equations are used to improve the accuracy of the predicted efficiency.

Inertial impaction occurs when a particle is unable to adjust itself quickly enough to the changing streamlines to continue to flow in the streamline and impacts on a fiber. Strauss [1975] gives an equation for the single fiber collection efficiency due to inertial impaction:

$$\eta_I = \psi^3 / \{ \psi^3 + (0.77\ \psi^2 + 0.22)\} \qquad (2.1)$$

The Stokes number, defined as the ratio of particle stopping distance to the fiber diameter, is used to theoretically determine the efficiency due to impaction:

$$\psi = (\rho\ v\ d_p^2\ C)\ /\ (18\ \mu\ d_f) \qquad (2.2)$$

where: ρ = density of particle
V = velocity
d_p = diameter of particle
C = slip correction factor
μ = gas viscosity = 1.81×10^{-4} poises
d_f = fiber diameter = 2×10^{-3} cm

Diffusion occurs when Brownian motion carries small particles outside the slipstream and into contract with a filter fiber. The single fiber collection efficiency due to diffusion is given by:

$$\eta_D = 6 (S_c)^{-2/3} (Re)^{-1/2} \quad (2.3)$$

The Schmidt number is defined as:

$$S_c = \mu / (\rho D) \quad (2.4)$$

The Reynolds number is defined as:

$$Re = (V \rho d_f) / \mu \quad (2.5)$$

The diffusion coefficient of a particle is given by:

$$D = (C T k) / (3 \pi \mu d_p) \quad (2.6)$$

where:

T = temperature
k = Boltzmann's constant (1.38×10^{-16} dyne-cm/K)

Interception occurs when a particle following the streamline comes within one particle radius of a fiber and is captured by the fiber because of its finite size. The parameter governing interception is the Kuwabara hydrodynamic factor. This includes the effect of distortion of the flow field around a fiber due to its proximity to other fibers. The equation for the collection efficiency due to interception is given by Hinds [1982]:

$$= \{1 / (2\,Ku)\}\ \{2(1+R)\ [\ln(1+R)] - (1+R) + [1 / (1+R)]\} \qquad (2.7)$$

where:

$$Ku = \text{Kuwabara factor} = \alpha_f - ((\ln \alpha_f) / 2) - (3 / 4) - (\alpha_f^2 / 4) \qquad (2.8)$$
$$R = d_p / d_f$$

where:

α_f = solidity (volume density) of filter = 0.03

The combined single fiber efficiency is given as the sum of the efficiencies of each collection mechanism:

$$\eta = \eta_I + \eta_D + \eta_R \qquad (2.9)$$

The theoretical collection efficiency of the filter (E) is then determined from the following equation given by Hinds [1982]:

$$E = 1 - e^{-(f \eta)} \qquad (2.10)$$

where:

$$f = 4\,\alpha_f h / \pi d_f \qquad (2.11)$$
h = depth of filter material = 5.08 cm. (2 in.)

2.7 Comparison Between Theory and Experiment

Using the equations presented in the previous section, the theoretical collection efficiency can be determined for the prefilter material. The theoretical curves are shown in Figure 2-8, at a velocity of 152 cm/s, and Figure 2-9, at a velocity of 53 cm/s, along with the experimental curve for both solid and liquid particles. Figure 2-8 includes the set of three data points from the solid particle mass loading tests and three data points from the liquid mass

loading tests in order to provide a more complete representation.

Clearly the theoretical graph in Figure 2.8 predicts a much higher penetration (lower efficiency) for all particle sizes less than about 5 μm, than is shown experimentally. For larger particle diameters nearly complete collection is predicted and observed. A similar trend is noticed at the lower velocity data in Figure 2.9. This discrepancy is probably due to the difference between an "ideal" and a real filter. The real filter does not have uniform fiber diameters; porosities or thickness. Clearly, using the theoretically determined efficiency based on these equations would result in a conservative over-estimate of the amount of material penetrating the prefilter of the AACS. For these reasons, the measured prefilter collection efficiency curve should be used for predicting the mass loading on the AACS. The results of these calculations predicting the AACS mass loading are presented in Section 4.0. The calculational methodology is detailed in Appendix B.

3.0 MASS LOADING TESTS

3.1 Experimental Descripti

A schematic of the mass loading experimental apparatus is shown in Figure 3-1, similar to the apparatus set up for the efficiency tests described in Section 2.1. The major difference was that a dewpoint hygrometer was used to monitor the humidity and the CNCs and LAS were not used. The mass loading experiments were conducted with solid particles, liquid droplets and a 50% mixture of solid and liquid particles by volume.

The desired aerosol was dispersed and mixed in a 1.5 m (60") long by 0.76 m (30") diameter vacuum/pressure vessel, with filtered dry room air. The aerosol was drawn through the 7.6 cm x 10.2 cm (3 in x 4 in) prefilter and a 3855.5 cm^2 (4.15 ft^2) HEPA filter by a blower. Due to the availability of only standard sizes of HEPA filters, this geometry simulates one prefilter for each HEPA filter as opposed to the actual AACS configuration of 20 prefilters for every 32 HEPA's. The nominal flow rate of 100,000 cfm for the AACS was simulated with a flow controller to regulate the volumetric flow rate through the blower providing a media velocity of 152 cm/s through the prefilter and 3 cm/s through the HEPA filter. The pressure differences across the prefilter and HEPA filter were monitored using two MKS pressure transducers accurate to 13.3 Pa. The particle size distribution of the aerosol was determined using a cascade impactor that sampled from the aerosol mixing chamber.

Before each test both the prefilter and HEPA filter were weighed on a top loading digital balance. The filters were loaded with challenge aerosols until a desired total pressure difference across both filters was achieved. When the given target pressure difference was reached, both filters were removed from the system and weighed again. The change in mass was used to determine the mass loading per unit filter area. For liquid aerosol mass loading tests, the prefilter and HEPA filter were weighed when the target ΔP was reached, then replaced into

the system and the test continued until the next ΔP was reached. This procedure was repeated until the final target ΔP was reached. In contrast to the liquid tests, the solid particle mass loading tests each had to be started from ΔP_0, removed and weighed at the target ΔP, and new filters used for the next target ΔP. This was required due to the change in particle cake structure caused by handling of the prefilters. The mass loading per unit area data was plotted against the difference between the final pressure drop and initial clean pressure drop. These results will be detailed in a later section.

3.2 Apparatus for Aerosol Generation

3.2.1 Liquid Particles

Four aerosol generators were used to generate liquid particles of three different sizes. A BGI Inc. 6-Jet Collision Atomizer was used to atomize a solution of 50% dioctyl phthalate (DOP) and 50% isopropyl alcohol generating particles with an MMAD of approximately 1.5 μm. To generate an aerosol with an MMAD below 1 μm, a 10% solution of DOP in isopropyl alcohol was atomized in a BGI 36-jet Collison atomizer. The principles of operation of this generator are the same as those of the 6-jet Collison atomizer described in Section 2.2.

To generate particles with an MMAD greater than 1.5 μm, an evaporation-condensation aerosol generator (Figure 3-2) was used in conjunction with a TSI Constant Output Atomizer (COA). The output aerosol of the COA was mixed with a hot vapor, and cooled. As the vapor cools, it condenses on the existing particles, forming an aerosol with an MMAD greater than 1.5 μm. The final aerosol size and concentration were a function of the size of the feed aerosol, flow rate of the aerosol, and the temperature gradient of the cooling vapor.

The fourth liquid generation technique used three Bennett ultrasonic nebulizers to generate an aerosol with an MMAD greater than 1.5 μm. The nebulizer consists of a piezoelectric crystal with a controlled amplitude of vibration oscillating in a water bath. The

water bath oscillates against a membrane which, in turn, vibrates the source solution (any liquid with the proper viscosity). The source solution is disrupted by the vibration, causing small droplets to be dispersed from the liquid surface. Air flows through this portion of the generator suspending these droplets as an aerosol. Particle size is dependent on the amplitude of vibration, solution concentration, and viscosity.

3.2.2 Solid Particles

Three distributions of solid particles were dispersed using a BGI Model WDF-II Wright dust feeder (Figure 3-3). Aluminum oxide powder was dispersed to produce the solid particle aerosol. The powder was uniformly packed into a stainless steel cup (1). A gear (5), driven by a motor, rotates the cup over the stationary cutter head and blade (3). The cup slowly descends as it turns, allowing the blade to "shave off" the powder which is then dispersed by incoming air into the aerosol mixing chamber. The output aerosol particle size is solely dependent on the size of the powder used down to a limit of about 0.1 μm.

3.3 Theory

3.3.1 Solid Particles

The simplest model for the relationship between mass loading and pressure difference across a given filter is the cake model:

$$\Delta P = \Delta P_o + \Delta P_c \qquad (3.1)$$

where:

ΔP = total pressure difference
ΔP_o = initial pressure difference across the clean filter
ΔP_c = pressure difference across the particle cake

and

$$\Delta P_o = K_1 V \qquad (3.2)$$

$$\Delta P_c = K_2 V M / A \qquad (3.3)$$

Thus,

$$K_2 = (\Delta P - \Delta P_o) A / V M \qquad (3.3a)$$

where:

K_1 = constant depending on filter parameters
K_2 = specific resistance of the cake
V = filter media gas velocity
M/A = mass of collected aerosol per unit area

This model describes the total pressure drop as the sum of the clean filter ΔP_0 and the ΔP_c across an independent particle cake. This model is easily applied to HEPA filters because the high efficiency causes a particle cake to rapidly form on the surface of the HEPA filter. This particle cake eventually becomes the primary filtration medium, its mass loading characteristics dominating the HEPA filter/cake combination. For a low efficiency filter, like the woven fiber prefilter, a particle cake never covers the entire surface of the prefilter (see Photo 1), most of the particles are removed inside the layers of the prefilter.

A more applicable model that accounts for particle collection throughout a porous filter is described by Bergman et al [1978]:

$$\Delta P = 64 \mu V h [(\alpha_f / d_f^2) + (\alpha_p / d_p^2)]^{1/2} [(\alpha_f / d_f + \alpha_p / d_p)] \qquad (3.4)$$

where:

ΔP = pressure difference across the filter
ΔP_o = initial pressure difference across the filter
μ = the viscosity of the carrier gas
h = the thickness of the filter
α_f = the volume density of the filter fibers
α_p = the volume density of the particles

If the volume density of the fibers is greater than the particle volume density, and if the fiber effective collection diameter is smaller than the particle structure's effective collection diameter, then Equation 3.4 can be simplified to :

$$\Delta P - \Delta P_o = [(64\ \mu\ V\ h\ (\alpha_f)^{1/2}) / d_f]\ [\alpha_p / d_p] \qquad (3.5)$$

These assumptions are typically true for HEPA filters but it is not clear if they can be considered true for the prefilter material. Assuming that they are applicable, Bergman's equation can then be written in terms of mass loading per unit area using the relationship,

$$M = \rho\ h\ A\ \alpha_p \qquad (3.6)$$

where:

M = the total mass
A = the surface area of the filter
ρ = the density of the particle

Combining Equations 3.5 and 3.6,

$$\Delta P - \Delta P_o = 64\ M\ \mu\ V\ (\alpha_f)^{1/2} /\ d_p\ d_f\ A\ \rho \qquad (3.7)$$

Equation 3.7 can be used to describe the increase in ΔP as a function of the mass loading per unit area and the gas velocity.

$$\Delta P - \Delta P_o / (M / A)\ V = 64\ \mu\ (\alpha_f)^{1/2} / d_p\ d_f\ \rho \qquad (3.8)$$

The left side of Equation 3.8 is identical to the experimentally determined value of K_2 in the cake model. Bergman's model can be used to define a theoretical value of a combined specific resistance as :

$$K_2 = 64\ \mu\ (\alpha_f)^{1/2} / d_p\ d_f\ \rho \qquad (3.9)$$

This second model for K_2 is dependent on the volume fraction of original fibers, and the original fiber diameter. Both of these quantities are difficult to quantify because of the nature of the prefilter. The volume fraction provided by the manufacturer is questionable in its

consistency as the filter is packed into a holder and may conceivably change as the filter is used, washed, and reused. This theory also introduces the concept of the effective collection diameter, which may or may not be equal to the actual fiber or particle diameter. However, this model does predict a linear relationship between the product of the diameter of the particle and the change in pressure difference, and the mass collected by the filter. As shown later, the limited data produced in this work is best described by a linear fit.

3.3.2 Liquid Particles

Mathematical models which predict the pressure difference across a filter challenged by a liquid aerosol are very sensitive to the geometry of the filter. Liew and Condor [1985] have developed a model describing the ratio of the pressure difference for a liquid coated filter compared to a clean dry filter:

$$\Delta P_{we} / \Delta P_o = A_1 [(d_f / \alpha_f h)^{.561} (A\ t \cos\phi / Q\ \mu)^{.477}] \qquad (3.9)$$

where:
- ΔP_{we} = the pressure difference across the wet filter in an equilibrium condition
- ΔP_o = the pressure difference across the dry filter
- A_1 = Liew and Condor correlation coefficient
- Q = the volumetric flow rate
- t = surface tension of the liquid
- ø = contact angle of the particle with respect to the fiber's surface
- A = area of the filter

As in the equations developed in Bergman's model, the effective fiber diameter is an uncertain quantity to define for the prefilter. In addition, the contact angle of the droplet with respect to the fiber is unknown. Furthermore, this model only describes the pressure difference across a prefilter that is in equilibrium between mass collected and mass removed by drainage. These difficulties limit the usefulness of the model.

The authors conclude that this model is valid when used for rough estimates of filters

with a packing density above 0.02. They admit its predictive accuracy is not high, but claim it[42] is a great improvement over assuming $\Delta P_w = \Delta P_o$, where ΔP_w = the pressure difference across the wet prefilter.

3.4 Mass Loading Results

3.4.1 Liquid Mass Loading Results

A graph of the results of the experiments measuring the mass loading as a function of the pressure difference across the prefilter for three different liquid aerosol distributions is given in Figure 3-4. Table V shows the relationships between the amount of mass collected on the prefilter, the change in pressure and efficiency of the prefilter. The pressure difference across the prefilter increased only slightly and the efficiency remained virtually constant as the mass loading on the prefilter increased. The slight variations in the pressure difference can be primarily accounted for by the resolution of the pressure transducer (minimum resolution is 13.3 kPa).

Observations of the prefilter assembly at low mass loadings indicated no signs of drainage. The conclusion is that all of the liquid simply wets the available fiber area with a thin film. As the mass loading on the prefilter increased, drainage of liquid from the prefilter was observed indicating that a maximum film thickness, resulting in a maximum mass loading can be attained. Continued liquid loading beyond the maximum results in an equilibrium, such that the mass of liquid collected equals the mass that drains from the prefilter material. No increase in the pressure difference across the prefilter was measured even after achieving equilibrium.

TABLE V

PREFILTER LIQUID MASS LOADING

TEST NUMBER	PARTICLE DIAMETER	$M_{Prefilter}$ (grams)	$\Delta P_{Prefilter}$ (Pascals)	PERCENT EFFICIENCY
1	1.79 µm	not taken	40.28	NOT TAKEN
2	1.37 µm	39.35	0.00	40.20%
3	1.35 µm	53.85	40.28	42.20%
4	1.57 µm	45.55	0.00	42.80%
5A	1.50 µm	14.80	53.70	38.70%
5B	1.50 µm	26.75	13.43	38.50%
5C	1.50 µm	32.50	26.85	38.00%
5D	1.50 µm	42.50	40.28	38.30%
6A	1.53 µm	7.40	0.00	14.50%
6B	1.53 µm	8.80	13.43	14.90%
6C	1.53 µm	10.85	0.00	14.90%
7A	1.59 µm	27.85	40.28	49.90%
7B	1.59 µm	44.85	53.70	46.60%
7C	1.59 µm	56.10	53.70	45.60%
7D	1.59 µm	59.35	67.13	42.00%
9A	3.98 µm	9.90	0.00	93.80%
9B	3.98 µm	14.50	0.00	95.70%
9C	3.98 µm	21.10	26.85	97.00%
9D	3.98 µm	27.65	0.00	99.50%
9E	3.98 µm	32.43	0.00	96.30%
9F	3.98 µm	36.68	0.00	95.30%
10A	3.58 µm	10.50	13.43	95.00%
10B	3.58 µm	26.35	13.43	93.90%
10C	3.58 µm	53.80	13.43	95.90%
10D	3.58 µm	75.10	0.00	95.50%
10E	3.58 µm	90.61	0.00	94.60%
12A	0.71 µm	1.30	13.43	13.70%
12B	0.71 µm	10.10	26.85	14.20%
12C	0.71 µm	12.55	40.28	14.40%
12D	0.71 µm	14.25	26.85	14.40%
12E	0.71 µm	16.25	26.85	14.30%

Under equilibrium conditions, liquid was observed on the ends of the fibers extending from the downstream face of the prefilter as well as a liquid coating found on the ductwork, downstream of the prefilter. No appreciable increase in mass loading was noted on the HEPA filter, thereby indicating that these re-entrained liquid droplets were very large and could not remain suspended in the gas stream. This conclusion is applicable to the AACS, assuming there is adequate distance (more than 6 inches) between prefilter and HEPA filter, so the re-entrained droplets can also be deposited on ductwork downstream from the prefilter. The data also indicates that the structure of this particular prefilter allows the assumption that ΔP is equal to ΔP_0 for all levels of liquid mass loading.

Figure 3-5 shows the relationship between mass loading and pressure difference across the HEPA filter for various liquid aerosols. For the liquid particle distribution of 3 μm, only a small amount of mass is collected on the HEPA filter with no change in the pressure difference. This is expected since the prefilter collects most of the larger aerosol particles as discussed previously in the Section 2. As the prefilter efficiency decreases with particle diameter, the HEPA is challenged by more liquid mass resulting in a constant increase in pressure difference as the HEPA filter is loaded. An unexpected result is the higher pressure difference shown for the 1.53 μm particles over the 0.71 μm particles at a given mass loading. It was anticipated that the liquid films produced around each fiber would be independent of initial droplet size.

It is interesting to note that during scoping tests, high pressure differences up to approximately 1473.6 Pa could be achieved with complete liquid saturation of the HEPA filter. Under these conditions, the HEPA filter ruptured. This is consistent with some observations made by Gunn and Eaton [1976] for the maximum pressure drop resulting in HEPA filter rupture.

3.4.2 Solid Mass Loading Results

Figures 3-6 and 3-7 summarize the experimental data examining the relationship between mass loading and pressure difference across the prefilter for solid aerosol particles. Figure 3-6 plots mass loading as a function of the pressure difference across the prefilter for each of the three particle sizes tested. Mass loading for a given pressure difference increases with particle size as expected from theory and as noted in earlier HEPA filter tests [Novick et al, 1990a].

The prefilter mass loading is plotted in Figure 3-7 as a function of the product of the change in pressure difference and particle size. A linear relationship was found to exist, consistent with the simplified Bergman model. A correlation coefficient of R = 0.936 was determined by a statistical fit to the data. The scatter in the data in Figures 3-6 and 3-7 is a result of the tests using 3.07 μm solid particles. For these tests, packing of the alumina oxide powder into the Wright dust generator (as described in Section 3.2.2) had to be achieved utilizing a hydraulic press instead of packing the dust manually as was done for the other solid particle tests. This was necessary to achieve a sufficiently tight packing of the dust into the stainless steel cup of the dust generator. However, this extra packing of the powder produced problems during some of the tests generating 3.07 μm particles causing the dust generator to operate intermittently. It is believed that the intermittent operation of the dust feeder, caused an increase in the scatter in that particular data set.

Replotting the data in terms of the specific resistance and the mass median particle diameter, Figure 3-8 shows the linear relationship for the three solid particle sizes tested. A correlation coefficient of 0.996 was obtained for the curve in Figure 3-8. The value for K_2 was determined by dividing the slope of each curve on the graph of Figure 3-6 by the filtration velocity and multiplying by the cross sectional area of the prefilter. The density was assumed to

velocity and multiplying by the cross sectional area of the prefilter. The density was assumed to be a constant since the same material, Al_2O_3, was used for all tests.

Figure 3-9 plots the data from each group of solid particle tests for different particle size distributions. HEPA filter mass loading is graphed as a function of the pressure difference. As particle size increases, a decrease is noted in the pressure difference as the HEPA filter becomes loaded. This effect is the same as that observed in earlier work [Novick et al, 1989,1990]. It should be noted that the particle sizes in the legend are for the aerosol size distributions challenging the prefilter. The actual particle size distribution challenging the HEPA filters were not measured, but can be calculated as described in Appendix B.

3.4.3 Mixed Solid and Liquid Mass Loading Results

While the previous tests on separate solid and liquid aerosols provide information on the mass loading -vs- pressure difference relationship for pure solid or pure liquid aerosols, it is not clear if these results provide limits on the rate of pressure increase with mass loading for any aerosol. It is possible that an accident scenario may release quantities of solid and liquid aerosols simultaneously. Therefore, a test was performed with the prefilter and HEPA filter material of the AACS, to determine if the envelope of specific resistances defined by the pure solid and pure liquid tests, also encompassed the pressure response to a combined liquid and solid aerosol mass loading.

The maximum output particle diameter of the Collison atomizer is an MMAD of 2.0 μm. An Al_2O_3 powder size was chosen to match the MMAD of the liquid (DEG) as close as possible. It was determined that the 1.0 μm Al_2O_3 powder had a measured MMAD of 2.23 μm with an uncertainty of ±0.24 μm. The atomizer and dust generator were set up to disperse equivalent volumes of aerosol for the test. Visually, the output of the dust generator was not as stable as

the atomizer. However, post test analysis indicated that equal volumes of material were dispersed. The measured MMAD of the mixed aerosol was found to average 2.5 μm. The results of the four filter loadings are presented in Figure 3.10. A linear least squares fit to the data gives a correlation coefficient of 0.94.

Due to inconsistencies of the Wright Dust Feeder output, the ratio of the masses of solid and liquid particles fluctuated during the experiment. The pressure difference measurements were sensitive to these fluctuations. When liquid aerosol was the dominant component, pressure difference was observed to decrease. Rapid increases in pressure difference occurred when the solid particles dominated the mixed aerosol. This effect may explain most of the inconsistencies and scatter in the results of these tests.

To determine how the mass loading from this combined test compared with the pure solid tests, the data was superimposed onto a graph including solid aerosol tests and liquid aerosol tests and shown in Figure 3-11. It is observed that the curve of solid/liquid mixture aerosol lies above all of the curves of the solid aerosols instead of in between the 1.3 μm and 3.07 μm tests, as would be expected if the solid test data provided a true limit on the maximum pressure increase for a given mass loading. The actual minimum mass loading limit cannot be determined from this single test. However, it is postulated that for large liquid to solid ratios in the aerosol, the prefilter will eventually become saturated with liquid and begin to drain. This drainage will also carry some solid particles with the liquid, eventually achieving an equilibrium condition between newly collected and drained material. As the liquid ratio approaches a pure liquid species, the pressure difference will remain constant as observed in the pure liquid tests.

The mass loading characteristics of the HEPA filter for the liquid/solid aerosol particle tests are shown in Figure 3-12. This graph shows the mass loading on the HEPA filter as a function of the pressure difference for the particle size distribution that penetrated the

prefilter. When this data is superimposed onto a graph including curves from the solid aerosol and liquid aerosol tests, the curve of the liquid/solid aerosol tracks the behavior of the 3.07 μm solid particle tests. These results are presented in Figure 3-13. One interpretation is that most of the liquid aerosol particles have been filtered by the prefilter and essentially only solid particles are being deposited on the HEPA filter. This could occur if the solid particle distribution has a greater geometric standard deviation than the liquid aerosol. This would result in more solid particles than liquid in the smaller size tail of the distribution. Another interpretation is that there was simply not enough mass penetrating the prefilter, to begin to see the effects of the liquid on the HEPA filter. As seen in Figure 3.5, about 0.005 g/cm^2 of liquid is necessary on the HEPA filter to begin to see an increase in the pressure.

4.0 CONCLUSIONS

The results of the efficiency and mass loading experiments can be used to model the behavior of the total aerosol mass collected by the AACS for a given pressure drop as a function of particle diameter. For solid particles, the basic equations used in the model include,

$$K_2 = (\Delta P - \Delta P_0) / ((M / A) V) \quad (4.1)$$

$$\Delta P_{AACS} = \Delta P_{HEPA} + \Delta P_{Prefilter} + (\Delta P_0)_{HEPA} + (\Delta P_0)_{Prefilter} \quad (4.2)$$

$$\text{EFFICIENCY} = M_{Prefilter} / (M_{Prefilter} + M_{HEPA}) \quad (4.3)$$

The equation for K_2 can be written for both the prefilter and HEPA filter. It is assumed that the initial pressure drop, ΔP_0, the filtration velocity and the effective filtration area are known for each filter. The total target pressure drop across the prefilter and HEPA filter portions of the AACS is given. The efficiency is taken from the correlation in Figure 2-8, based on a given or calculated MMAD. K_2 for the prefilter is taken from the correlation in Figure 3-8. K_2 for the HEPA filter is given by the equation fit to the data given in Figure B-1. The values for K_2 are

determined based on a given or calculated MMD. To convert between MMD and MMAD, the particle density must be known or given. This leaves four unknowns, ΔP_{HEPA}, $\Delta P_{Prefilter}$, M_{HEPA}, and $M_{Prefilter}$ to be solved by the four equations. The total AACS mass is simply the sum of M_{HEPA} and $M_{Prefilter}$.

Assuming a target pressure difference of 1750 Pa across the two filter components of the AACS, Figure 4-1 plots the predicted total mass collected by the AACS as a function of solid particle size. The filtration velocities used (Prefilter = 176 cm/s, HEPA = 2.54 cm/s) correspond to a volume flow of 120,000 cfm through the AACS. A final total pressure difference of 1750 Pa was used to represent 7 inches of water across the prefilter and HEPA filters of the AACS. In the small particle region the AACS mass is limited by the specific resistance of the HEPA filter. As the particle diameter is increased, the specific resistance of the prefilter becomes dominant. An example calculation describing the method of obtaining each data point in Figure 4-1, is given in Appendix B.

In order to determine the usefulness of this model, Table VI compares the predictive model results for solid particles with scaled Al_2O_3 experimental results. The average difference between the AACS mass predicted from calculations and the AACS mass extrapolated from the experimental data is -5.3%, with a standard deviation of ±20.5%.

Figure 4-2 plots the predicted AACS mass loading against the expected AACS mass loading based on extrapolation of these experimental results. Unfortunately, this is not a completely independent comparison because the experimental mass loading data is used to determine K_2 for the prefilter. However, the remaining parameters are independent and lead to the conclusion that relatively accurate predictions of AACS mass loading can be made as a function of postulated particle diameter and density.

TABLE VI

AACS MASS LOADING PREDICTED AND EXPERIMENTAL RESULTS

TOTAL ΔP (Pa)	MMAD (μm)	CALCULATED EFFICIENCY	MEASURED EFFICIENCY	AACS MASS Predicted from Calculations	AACS MASS Extrapolated from Experiments	% DIFFERENCE Between Predicted & Extrapolated
930.00	3.34	0.98	0.981	157.23	144.23	-9.01%
1488.00	3.16	0.98	0.935	281.28	325.80	13.66%
1608.00	3.13	0.98	0.968	280.95	231.54	-21.34%
2405.00	3.13	0.98	0.944	492.29	477.54	-3.09%
1953.00	2.65	0.97	0.975	306.03	404.82	24.40%
1143.00	1.38	0.85	0.815	51.97	62.78	17.22%
2405.00	1.35	0.84	0.834	176.65	183.55	3.76%
1927.00	1.21	0.81	0.825	119.02	117.81	-1.03%
1422.00	1.21	0.81	0.820	78.33	88.70	11.69%
957.00	0.99	0.74	0.695	35.53	29.76	-19.39%
1355.00	1.00	0.74	0.698	61.48	51.56	-19.24%
2365.00	0.83	0.66	0.625	107.03	92.20	-16.08%
2047.00	1.02	0.75	0.611	108.64	71.73	-51.46%

AVERAGE % DIFFERENCE : -5.3%
STANDARD DEVIATION : ±20.5%

The same type of model can be developed for predictions of liquid mass loaded onto the AACS. The liquid model uses equations 4.2 and 4.3 as before but equations cannot be written for K_2 because no cake is formed. Instead, Figure 3-5 was used to determine an average mass loading for a liquid at a given ΔP regardless of particle diameter. In addition, $\Delta P_{Prefilter}$ is assumed to be zero, based on the results presented in Figure 3-4. This results in only two unknowns, ΔP_{HEPA} which can now be calculated directly from equation 4.2, given a target pressure and the initial pressure drops across the filters, and $M_{Prefilter}$ which can be calculated directly from equation 4.3 after determining the efficiency from Figure 2-8. As before, the filtration velocity and filtration areas must be known and the particle diameter and density either given or assumed. An example calculation is provided in Appendix B.

Figure 4-3 plots the predicted liquid mass loading as a function of particle diameter using this model. The higher mass loading in the small particle region is dominated by the HEPA filter and mass loading is believed to be due to a wicking phenomenon that pulls the liquid into the fibers, coating each with a thin film. The ΔP of the HEPA increases due to the film bridging across adjacent fibers, restricting the available flow passages. As the particle diameter is increased, the prefilter efficiency increases but the total ΔP is still controlled solely by the HEPA. Eventually, very little aerosol reaches the HEPA filter so the total mass collected by the AACS becomes limited only by the capacity of the prefilter collection drain. No comparison is made between model and extrapolated values because too many of the parameters are common to both methods.

Figures 4-1 and 4-3 present predictions of the mass loading on the AACS as a function of particle size. The accuracy of these predictions appears to be better than 25% which is significantly better than other methods of estimation. These graphs represent the boundary

cases of mass loading on the AACS for pure solid aerosols or pure liquid aerosol, but do not necessarily represent the limits of mass loading for a mixed solid and liquid aerosol. Because only one series of tests for solid/liquid particles were done, for a single particle size distribution, predictions cannot be made as to the minimum mass limit of the AACS for a given pressure drop as a function of particle diameter. This minimum mass limit should be a function of the solid to liquid volume ratio eventually approaching the pure liquid limit as the ratio approaches zero.

APPENDIX A

EXPERIMENTAL PROCEDURES FOR THE EFFICIENCY TESTS

The specific data acquisition steps for prefilter efficiency measurements are outlined as follows.

- Twelve, double thickness prefilter pieces were loaded into the prefilter holder with thin gaskets between each. The prefilter holder was mounted in place within the test apparatus. An 8 in. x 10 in. HEPA filter was secured into its holder.

- The selected aerosol generator was filled with the appropriate solution, as discussed in Section 2.3. Pressurized dry, clean air was supplied to the generator inlet causing the solution to be atomized and aerosol particles of the appropriate size range to flow into the aerosol mixing chamber. In the tests where the electrostatic classifier was used, the voltages set on the classifier determined the particle size output into the chamber.

- As soon as aerosol was flowing freely into the mixing chamber, the exhaust air blower was turned on to pull the aerosol from the mixing chamber through the prefilter and HEPA filter. For tests using mass equivalent analysis, the test was run for a length of time appropriate to achieve adequate mass loading on the filters. For tests involving the CNCs and the particle counting method of analysis, at least 4, one minute timed readings of the particle count were done over a 30 minute time period.

- Particle diameters were measured or verified by Laser Spectrometer (LAS 250x)[54] and/or a cascade impactor. Several measurements were taken during most tests to confirm the stability of the output particle diameter.

- Upon completion of the test, the pressurized gas to the aerosol generator was turned off and the exhaust air blower was turned off. For the tests using the CNC particle count method, the prefilters were removed, cleaned and dried, and the HEPA filter was replaced. For tests using the mass equivalent method of analysis, the prefilters and HEPA filter were carefully removed and rinsed as discussed in Section 2.4, Analysis of Collected Particles.

- The procedure was then repeated for the next particle size. This procedure was the same for both solid and liquid particles.

APPENDIX B

CALCULATIONS FOR DETERMINING THEORETICAL MASS ON THE AACS

B.1 Solid Particles

The K_2 values used in the calculations were obtained from graphs of K_2 versus the inverse of the MMAD of solid particles, Figures B-1 for the HEPA filter and Figure 3-8 for the prefilter. For the HEPA filter, $K_{2H} = -1.586 \times 10^5 + 0.9494/D$. For the prefilter, $K_{2P} = 4.427 + 0.0001103/D$. From Section 4.0,

$$K_2 = (\Delta P - \Delta P_o) \; / \; ((M/A) \; V) \qquad (4.1)$$

$$\Delta P_{AACS} = \Delta P_{HEPA} + \Delta P_{Prefilter} + (\Delta P_0)_{HEPA} + (\Delta P_0)_{Prefilter} \qquad (4.2)$$

$$EFFICIENCY = M_{Prefilter} \; / \; (M_{Prefilter} + M_{HEPA}) \qquad (4.3)$$

Substituting the experimental HEPA correlation for K_2 into Equation 4.1, gives

$$K_{2H} = (\Delta P_H - (\Delta P_o)_H) \; / \; ((M/A)_H \; V_H) = -1.586 \times 10^5 + 0.9494/D \qquad (B.1)$$

and substituting the prefilter correlation for K_2 into Equation 4.1, yields

$$K_{2P} = (\Delta P_P - (\Delta P_o)_P) \; / \; ((M/A)_P \; V_P) = 4.427 + 0.0001103/D \qquad (B.2)$$

where $(\Delta P_0)_P$ = pressure difference across clean prefilter
ΔP_P = final pressure difference across prefilter
$(\Delta P_0)_H$ = pressure difference across HEPA filter
ΔP_H = final pressure difference across HEPA filter

Initial or known values include:

Total pressure difference of AACS:	$\Delta P_{AACS} = 1750$ Pa
Initial pressure difference across HEPA filter:	$(\Delta P_0)_H = 228.2$ Pa
Initial pressure difference across prefilter:	$(\Delta P_0)_P = 187.9$ Pa
Surface area of HEPA filter:	$A_H = 2229.7$ m^2
Surface area of prefilter:	$A_P = 32.12$ m^2
Velocity through HEPA filter:	$V_H = 0.0254$ m/s
Velocity through prefilter:	$V_P = 1.76$ m/s

solving equations B.1 and B.2 for the pressure difference across the HEPA filter, ΔP_H, and the pressure difference across the prefilter, ΔP_P, yields

$$\Delta P_H = -1.807\ M_H + 1.082 \times 10^{-5}\ M_H\ (1/D_H) + 228.2 \qquad (B.3)$$

$$\Delta P_P = 0.2427\ M_P + 6.027 \times 10^{-6}\ M_P\ (1/D_P) + 187.9 \qquad (B.4)$$

where M_P = mass collected on prefilter
M_H = mass collected on HEPA filter
D_P = particle size distribution challenging the AACS prefilter
D_H = particle size distribution challenging the AACS HEPA filter

Substituting into Equation.4 2 gives,

$$1750 = -1.807\ M_H + 0.2427\ M_P + 1.082 \times 10^{-5}\ M_H\ (1/D_H) + 6.027 \times 10^{-6}\ M_P\ (1/D_P) + 416.1 \qquad (B.5)$$

Rearranging equation 4.3 and solving for the total mass on the AACS HEPA filters,

$$M_H = M_P\ (1-E) / E \qquad (B.6)$$

where E = Efficiency

Equation B.6 can be substituted directly into Equation B.5 to give,

$$1750 = -1.807\ (M_P\ (1-E)/E) + 0.2427\ M_P + 1.082 \times 10^{-5}\ (1/D_H)\ (M_P(1-E)/E) + 6.027 \times 10^{-6}\ (1/D_P)\ M_P + 416.1 \qquad (B.7)$$

Solving for the total AACS mass on the prefilters yields,

$$M_P = 1333.9 / (-1.807\ ((1-E)/E)) + 0.2427 + 1.082 \times 10^{-5}\ (1/D_H)\ ((1-E)/E) + 6.027 \times 10^{-6}\ (1/D_P)) \qquad (B.8)$$

Efficiency is determined using the equation from the least squares fit to the data in Figure 2-8.

$$\text{norm}(x) = (\ln\ (y / 0.720)) / 0.712 \qquad (B.9)$$

where x = Efficiency
y = particle size (MMAD)

The efficiency is determined from the value of norm(x) using the Normal Probability Function Table (for example see pg. 580 of the CRC Standard Mathematical Tables 17th Edition).

The MMD of particles collected on the prefilter, D_P, is determined by dividing the MMAD by the square root of the density.

The MMAD of the particle distribution challenging the HEPA filter, is calculated by operating on the aerosol distribution challenging the prefilter with the prefilter efficiency as a function of particle diameter and is summarized in Table B.1. Since the original prefilter challenge aerosol was measured with a cascade impactor, the cut points of the impactor stages defined the segments to be used in calculating the HEPA filter challenge aerosol distribution (Table B.1 Column 1). The MMAD of the prefilter challenge aerosol was assumed to have a geometric standard deviation of 2. The relative mass in each segment is determined from a graph of the chosen MMAD with $\sigma_g = 2$ (Table B.1 Column 4).

The efficiency for each segment is calculated by substituting the cut point (ECD) values for y in Equation B.9 and solving for norm(x) (Table B.1 Column 2). The efficiency is determined from the Normal Probability Function Table (Table B.1 Column 3). The resulting efficiency for each segment is multiplied by the relative mass in that segment to give the amount of mass in that segment that challenges the HEPA filter (Table B.1 Column 5). After calculating a new mass for each segment (Table B.1 Column 6), the MMAD of the distribution is calculated by standard interpolation techniques. D_H, or the MMD of the distribution challenging the HEPA filter, is the MMAD divided by the square root of the particle density. D_p is the MMD of the prefilter challenge distribution. Substitution into Equation B.8 provides a prediction for the mass collected on the prefilter. When this result is substituted into Equation B.6, the mass on the HEPA filter is obtained. Using the calculated values of D_H, D_P, and E, a table of M_H and M_P was generated. The sum of these masses is the total mass collected on the AACS for solid aerosols at the initially given particle diameter.

$$M_{AACS} = M_{HEPA} + M_{Prefilter} \quad (B.10)$$

58

Figure 4-1 plots the predicted total mass collected by the AACS providing a total pressure drop of 1750 Pa, as a function of the mass median aerodynamic diameter. An example calculation for a 1 μm MMAD aerosol distribution with a σ_g equal to 2, is provided in the next section.

Example of calculations for determining theoretical mass on AACS

Let MMAD = 1.0 μm. Equations B-5 and B-6 are used to calculate the mass.

$$M_P = 1333.9 / -1.807 (1-E / E) + 0.2427 + 1.082 \times 10^{-5} (1/D_H) (1-E/E) + 6.027 \times 10^{-6} (1/D_P)$$

and

$$M_H = M_P (1-E) / E$$

Efficiency (E) is calculated using Equation B-7,

$$norm(x) = \ln (y/0.720) / 0.712 \quad (B.11)$$

$$= \ln (0.1/0.720) / 0.712 = 0.461$$

From Normal Probability Function Table on pg. 581 of CRC Standard Math Tables,

$$x = 0.461 \qquad F(x) = 0.6772 = E$$

To calculate D_P,

D_P = MMAD / $\rho^{1/2}$, where ρ = 3.90, the density for aluminum oxide

= $1.0 / 3.90^{1/2}$ = 0.51 μm

To calculate D_H, the ECDs of the 47 mm impactor are used.

TABLE B.1

CALCULATIONAL METHODOLOGY FOR DETERMINING D_H

ECD	norm(x)	Calc Prefilter Efficiency	Normalized Mass Dist ($D=1\mu m$, $\sigma_g=2$)	Calc Efficiency x Normalized Mass	New Dist Function for D_H
7.99	3.40	0.001	0	0	0
4.63	2.66	0.004	0	0	0
2.68	1.91	0.03	6.5	0.195	0.43%
1.55	1.15	0.125	20.0	2.5	5.51%
0.91	0.42	0.337	29.5	9.942	21.92%
0.53	-0.34	0.633	25.5	16.142	35.59%
0.31	-1.1	0.864	14.0	12.096	26.67%
0.10	-2.6	0.995	4.5	4.478	9.87%

TOTAL = 45.35

ECD	Cumulative Mass Fraction (% greater than ECD)
7.99	0
4.63	0
2.68	0.43%
1.55	5.94%
0.91	27.86%
0.53	63.46%
0.31	90.13%
0.10	100.0%

Using interpolation,

$$y - y_2 = [(y_2 - y_1) / (x_2 - x_1)] (x - x_2)$$

where, y_1 = % value under 50%
y_2 = % value over 50%
x_2 = ECD value of y_2
x_1 = ECD value of x_2
y = 50%
x = corresponding value to y

ECD_{50} = 0.67 μm

Therefore,

$$D_H = 0.67 / 3.90^{1/2} = 0.34 \ \mu m$$

Using E, D_P, and D_H to solve Equations B-5 and B-6,

M_P = 50.4 kg

M_H = 24.0 kg

M_{AACS} = 74.5 kg

The predicted values for M_{AACS}, for the assumptions and conditions noted above are plotted versus the MMAD in Figure 4-1, this particular data point being (74.5, 1.0).

B.2 Liquid Particles

Mass loading of liquid particles as a function of particle size for a pressure difference increase of 1750 Pa across the prefilter and HEPA filter element of the AACS was determined by combining equation 4.3, B.10 and B.12

$$\text{Efficiency} = M_{Prefilter} / (M_{Prefilter} + M_{HEPA}) \quad (4.3)$$

$$M_{Total\ AACS} = M_{HEPA} + M_{Prefilter} \quad (B.10)$$

$$M_{Prefilter} = (\text{Efficiency})\, M_{HEPA} / (1 - \text{Efficiency}) \quad (B.12)$$

which gives

$$M_{Total\ AACS} = M_{HEPA} + (\text{Efficiency})\, M_{HEPA} / (1 - \text{Efficiency}) \quad (B.13)$$

$$M_{Total\ AACS} = M_{HEPA} / (1 - \text{Efficiency}) \quad (B.14)$$

M_{HEPA} is determined by interpolating between the two curves in Figure 3-5. The average mass loading per unit area of the HEPA filter, for a pressure difference of 1750 Pa, is determined to be 0.019 grams/cm^2. Since the total area of the HEPA filter media in the AACS is 22,297,000 cm^2, the amount of mass the HEPA filters in the AACS collect is

$$M_{HEPA} = (0.019\ g/cm^2)(22{,}297{,}000\ cm^2) = 428\ kg$$

Equation B.14 is then used to determine the total AACS mass loading. The efficiency is determined as a function of particle size from equation B.11. For a particle size of 1 μm, the prefilter efficiency is 0.68 (see Appendix B.1). When the AACS is loaded to a pressure difference of 1750 Pa across the prefilters and HEPA filters by an aerosol having an MMAD of 1 μm, the total mass collected on the AACS is :

$$M_{Total\ AACS} = 428\ kg / (1 - 0.68) = 1337.5\ kg$$

The methodology described above was used to generate the AACS mass loading predictions given in Figure 4-3.

REFERENCES

Bergman, W., Taylor, R.D., Miller, H.H., Biermann, A.H., Hebard, H.D. da Roza, R.A., Lum, B.Y., "Enhanced filtration program at LLNL. A Progress Report" 15th DOE Nuclear Air Cleaning Conference, CONF-780819, Boston, [1978].

Gunn, C.A. and Eaton, D.M., "HEPA Filter Performance Comparative Study", 14th ERDA Air Cleaning Conference, CONF 760822, [1976].

Hinds, W. C., Aerosol Technology- Properties, Behavior, & Measurement of Airborne Particles, John Wiley & Sons, Inc., [1982].

Liew, T.P., and Condor, J.R., J. Aerosol Science, Vol. 16, No. 6, pp 497-509, [1985].

Novick, V. J. and Higgins, P. J., "Phase 1 Characterization of the Hepa Filter Media used in the Airborne Activity Confinement System at the Savannah River Site", WSRC-RP-89-793, [1989].

Novick, V.J., Abrahamson, C.A., and Richardson, W.B., "Relationship Between the Pressure Drop Across the Savannah River Site's HEPA Filter Material and Aerosol Mass Loading", WSRC-RP-90-779, [1990a].

Novick, V.J., Higgins, P.J., Dierkschiede, B., Abrahamson, C, and Richardson, W.B. , "Efficiency and Mass Loading Characteristics of a Typical HEPA Filter Media Material", 21st DOE Nuclear Air Cleaning Conference, [1990b].

Petry, S.F., et al, "L-Area Ventilation Tests-1984", SRL Report DPST-85336, [1985].

Strauss, W., Industrial Gas Cleaning, Pergamon Press, [1975].

Tinnes, S.P. and Petry, S.F., "Systems Analysis-Airborne Activity Confinement System of the Savannah River Production Reactors", SRL Report DPSTSY-100-10, [1986].

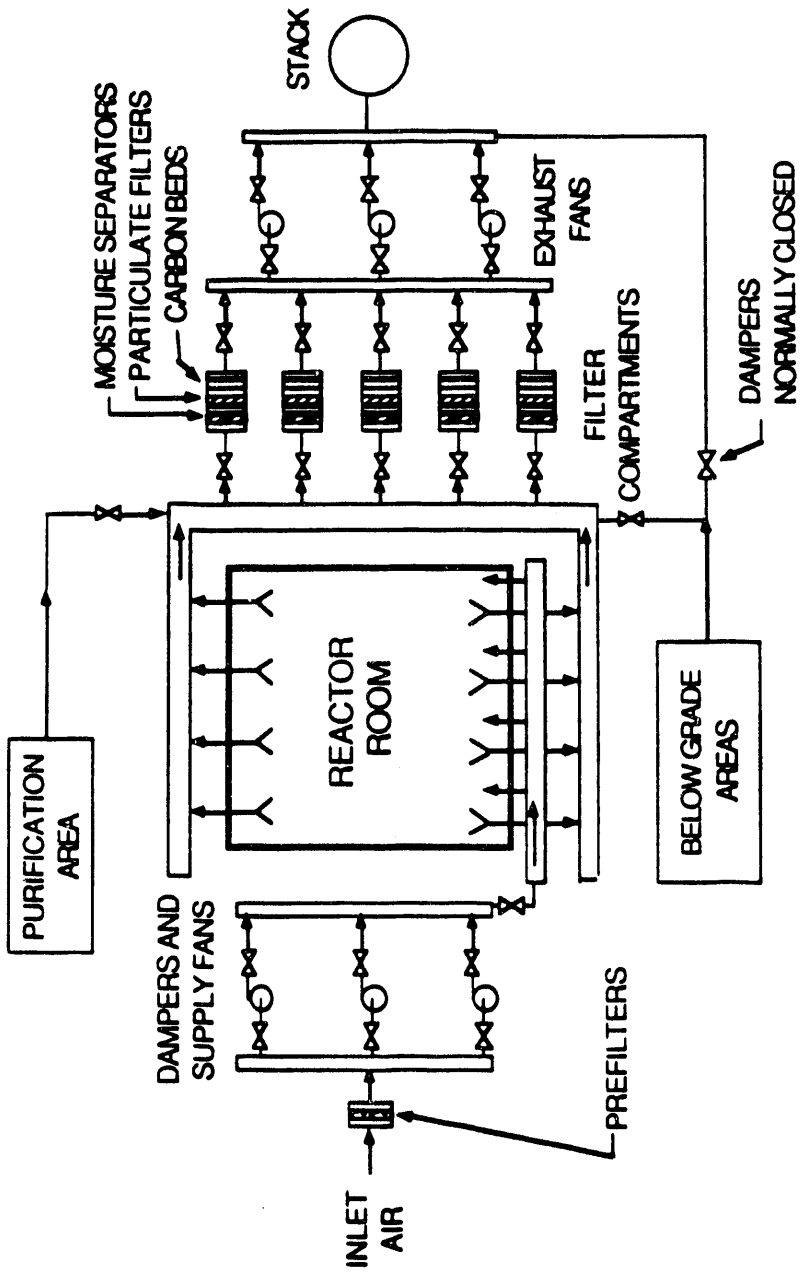

FIGURE 1-1: Schematic of the Airborne Activity Confinement System (AACS).

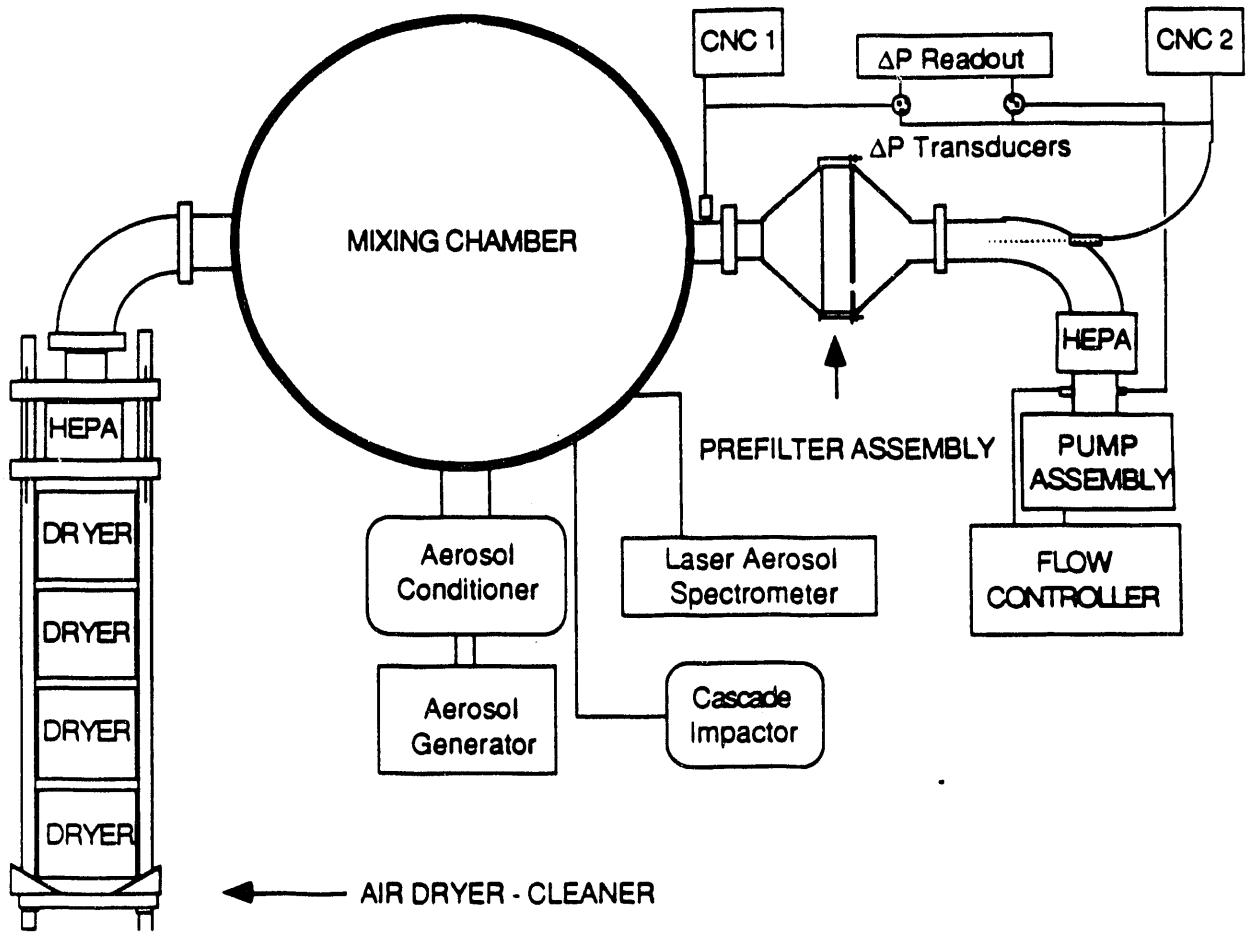

FIGURE 2-1 Experimental apparatus for Efficiency Tests for both solid and liquid particles.

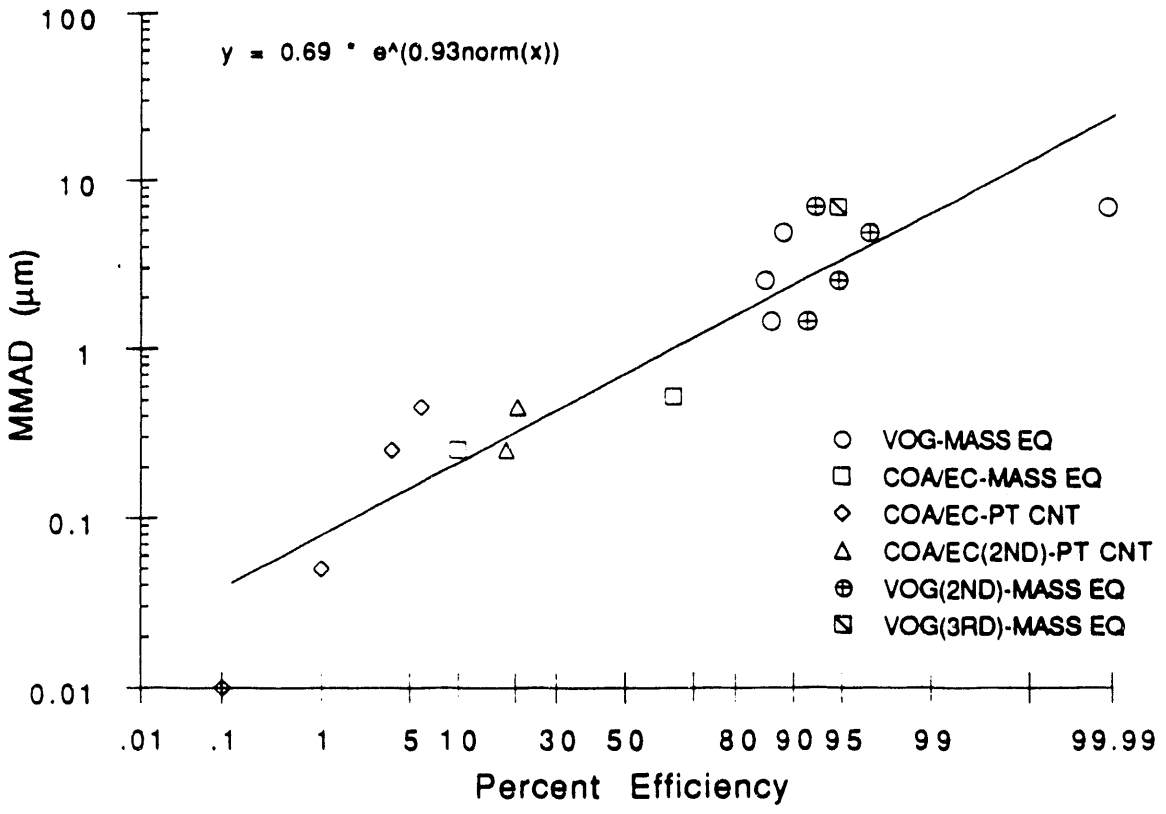

FIGURE 2-2 Efficiency -vs- particle diameter for solid particles for SRS prefilter material at a face velocity of 152 cm/s. Two aerosol generation methods were used to obtain the different particle sizes. Two methods of analysis were used, mass measurement (MASS EQ) using fluorimetry and particle counting (PT CNT).

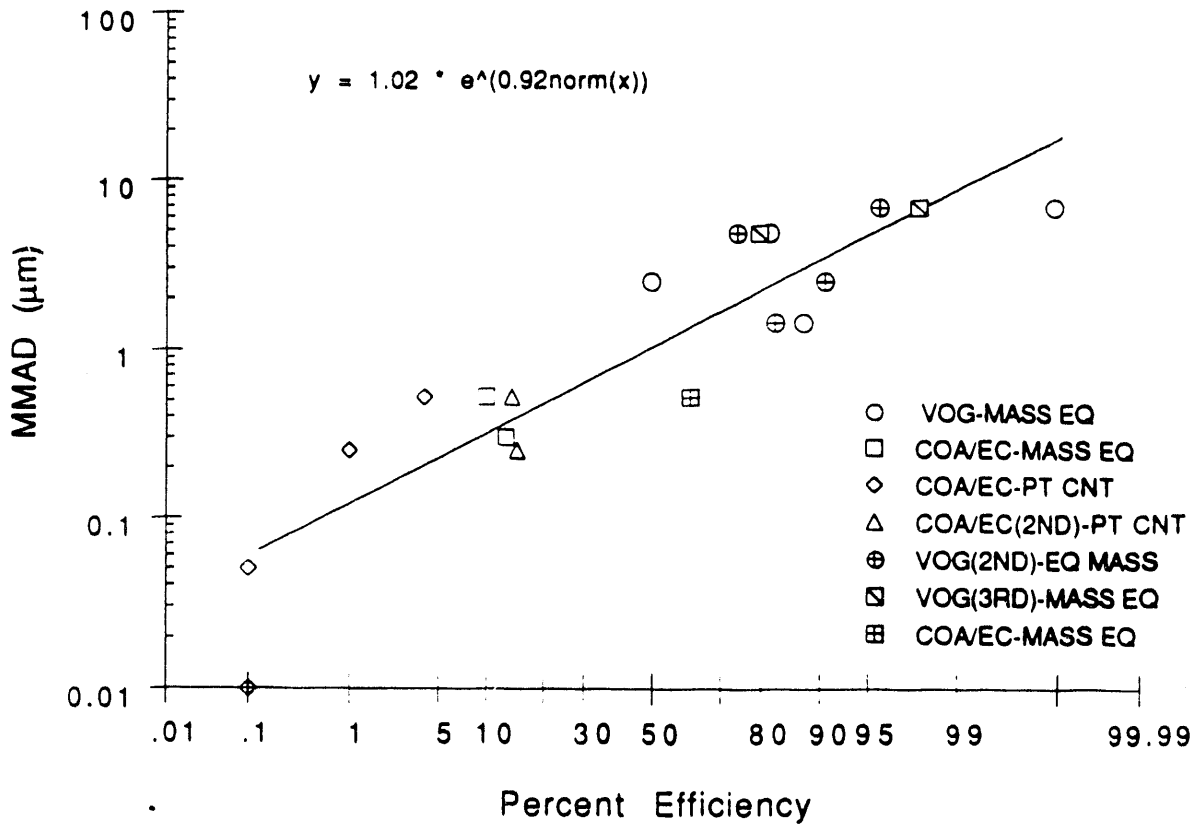

FIGURE 2-3 Efficiency -vs- particle diameter for solid particles for SRS prefilter material at a face velocity of 53 cm/s. Two aerosol generation methods were used to obtain the different particle sizes. Two methods of analysis were used, mass measurement (MASS EQ) using fluorimetry and particle counting (PT CNT).

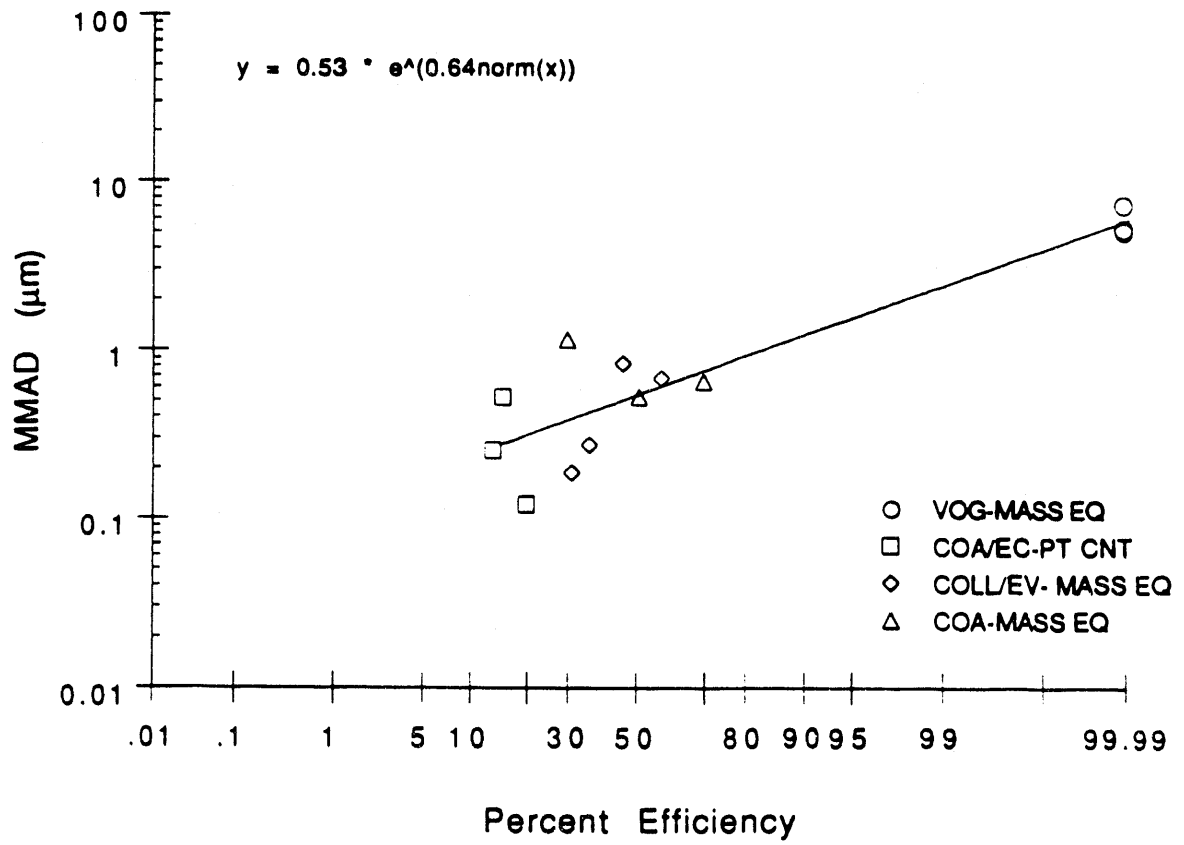

FIGURE 2-4 Efficiency -vs- particle diameter for liquid particles for SRS prefilter material at a face velocity of 152 cm/s. Four aerosol generation methods were used to obtain the different particle sizes. Two methods of analysis were used, mass measurement (MASS EQ) using fluorimetry and particle counting (PT CNT).

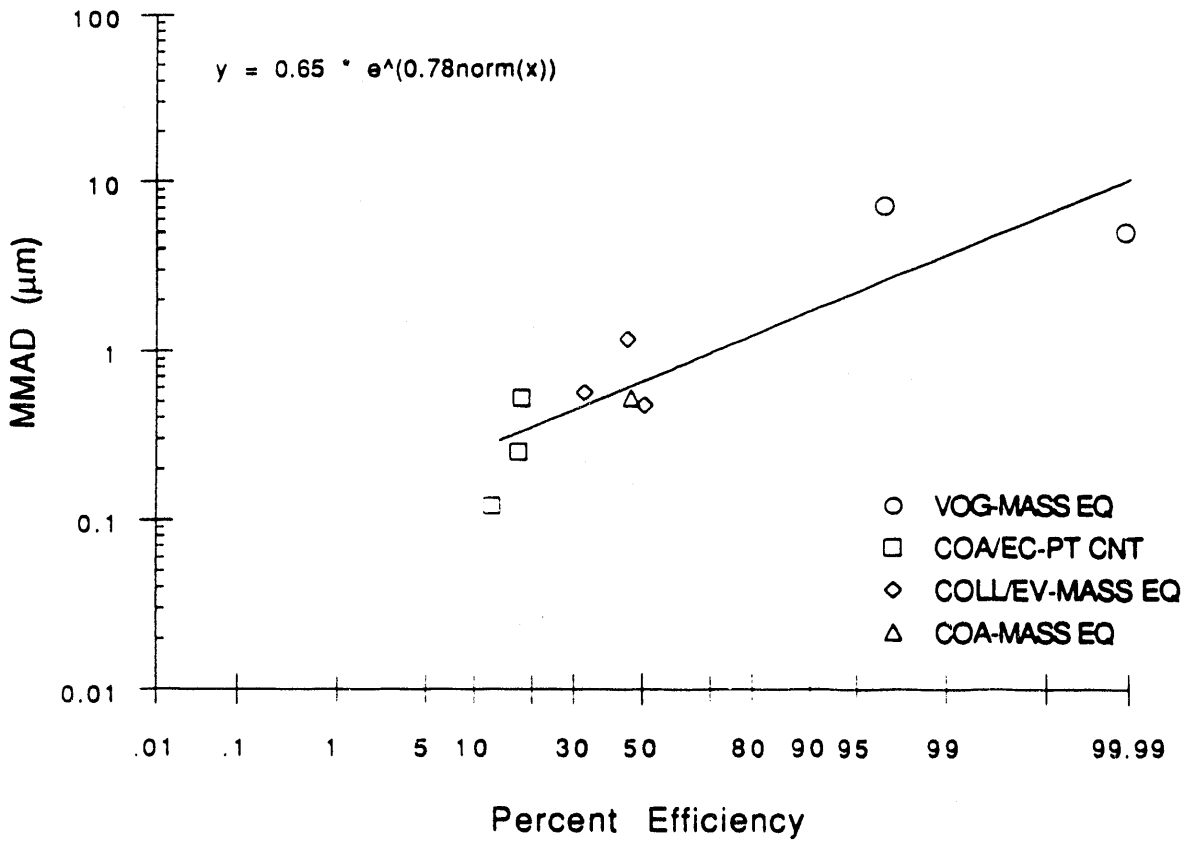

FIGURE 2-5 Efficiency -vs- particle diameter for liquid particles for SRS prefilter material at a face velocity of 53 cm/s. Four aerosol generation methods were used to obtain the different particle sizes. Two methods of analysis were used, mass measurement (MASS EQ) using fluorimetry and particle counting (PT CNT).

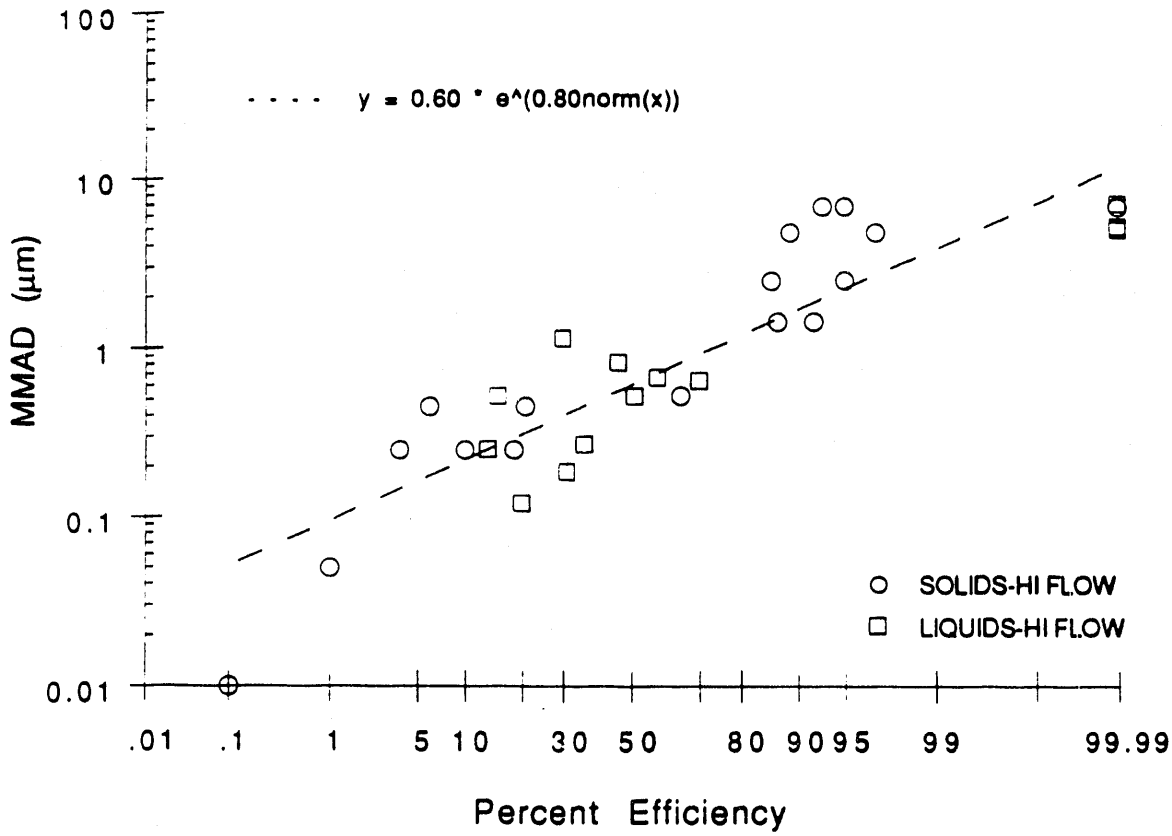

FIGURE 2-6 Experimental data of efficiency -vs- particle diameter for solid and liquid particles for SRS prefilter material at a face velocity of 152 cm/s.

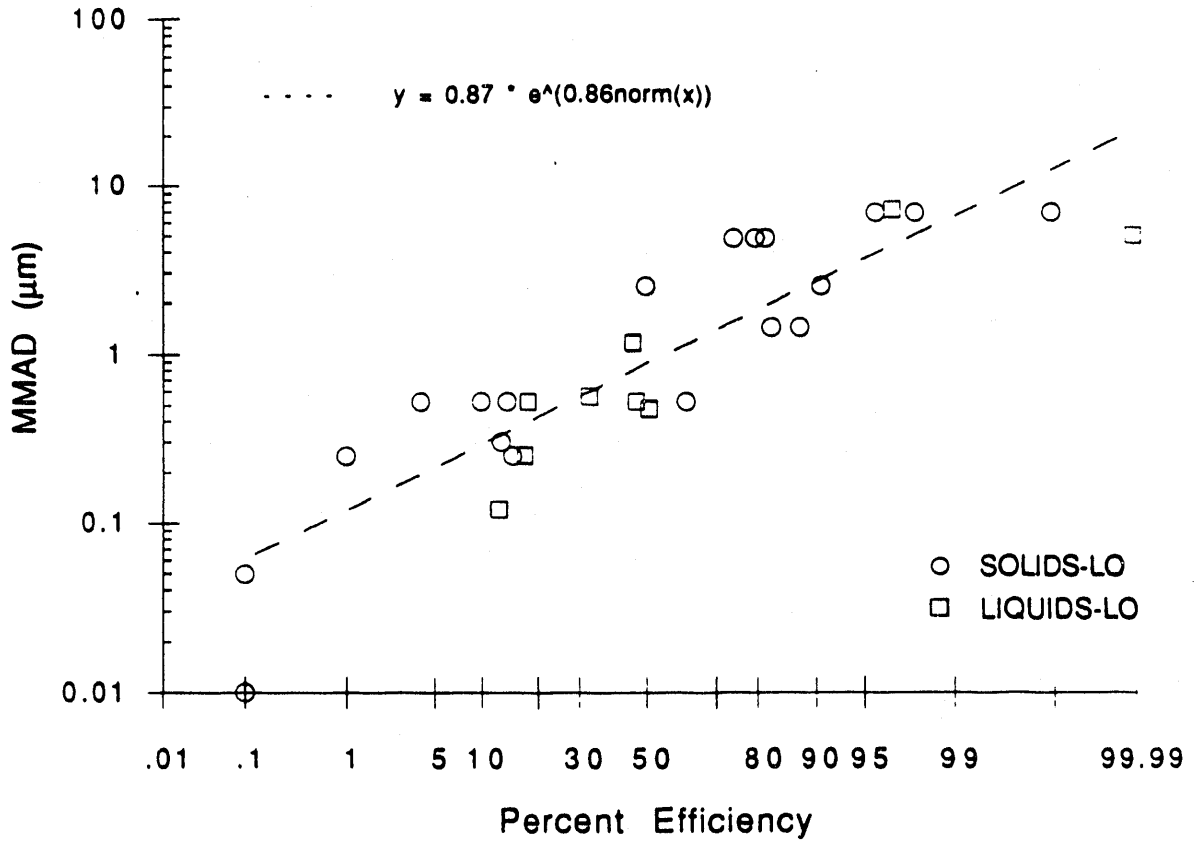

FIGURE 2-7 Experimental data of efficiency -vs- particle diameter for solid and liquid particles for SRS prefilter material at a face velocity of 53 cm/s.

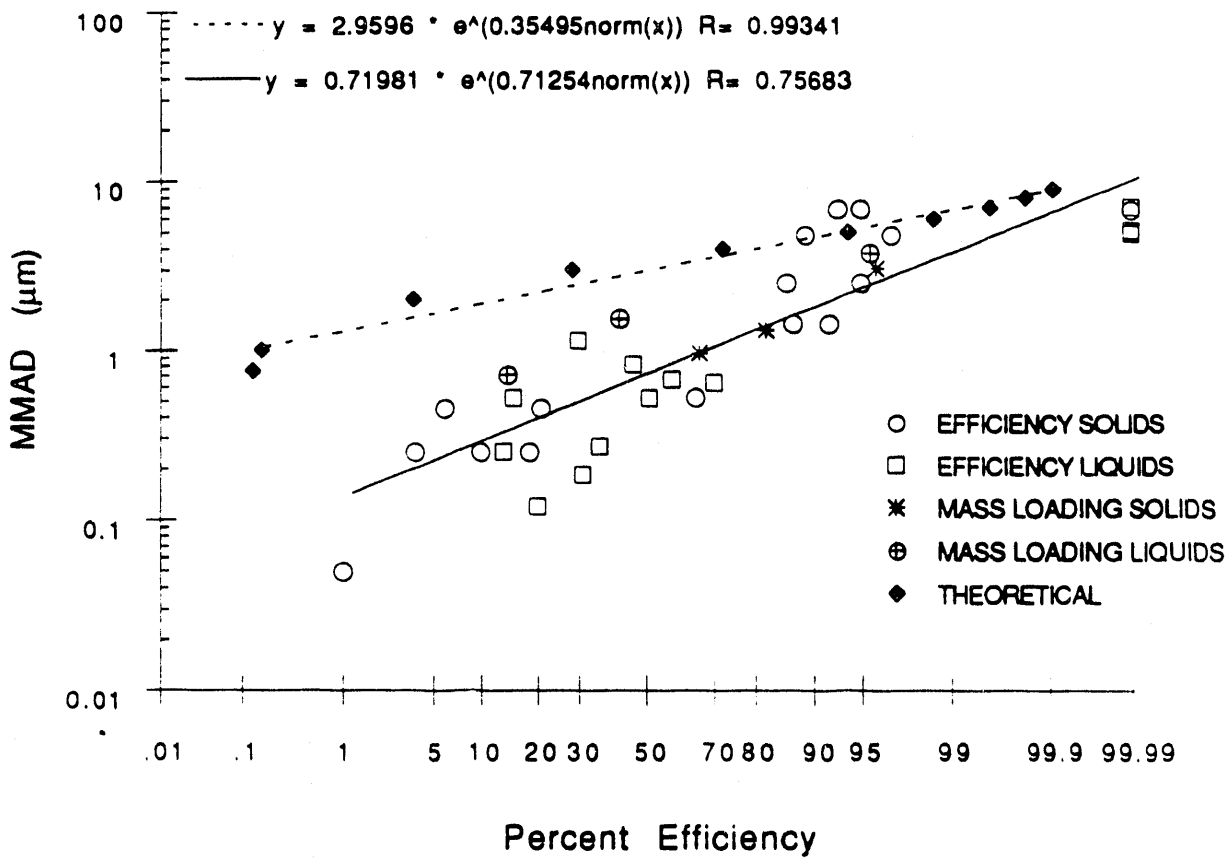

FIGURE 2-8 Theoretical and experimental collection efficiency curves for particles for SRS prefilter material at a face velocity of 152 cm/s. Experimental particle diameters are both solid and liquid particles. Both efficiency and mass loading data is included in this graph.

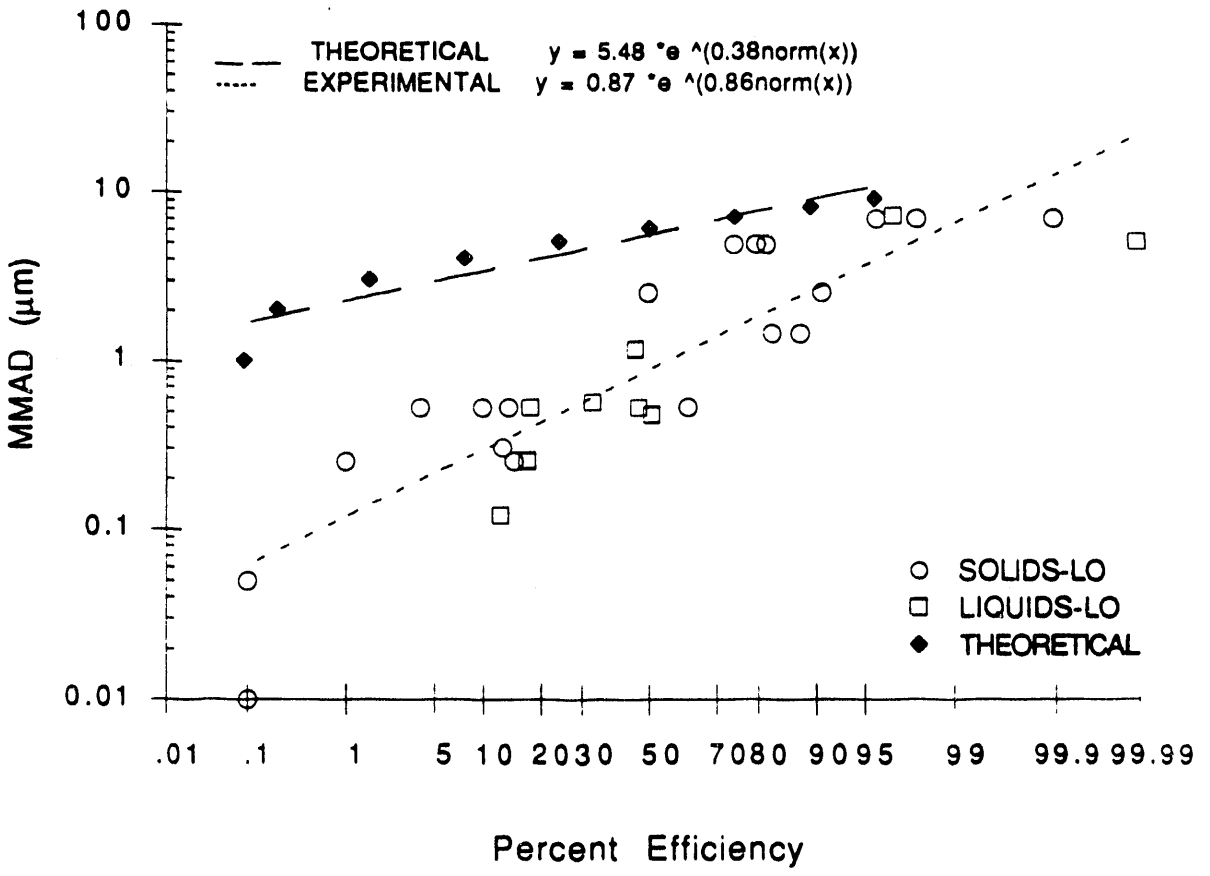

FIGURE 2-9 Theoretical and experimental collection efficiency curves for particles for SRS prefilter material at a face velocity of 53 cm/s. Experimental particle diameters are both solid and liquid particles.

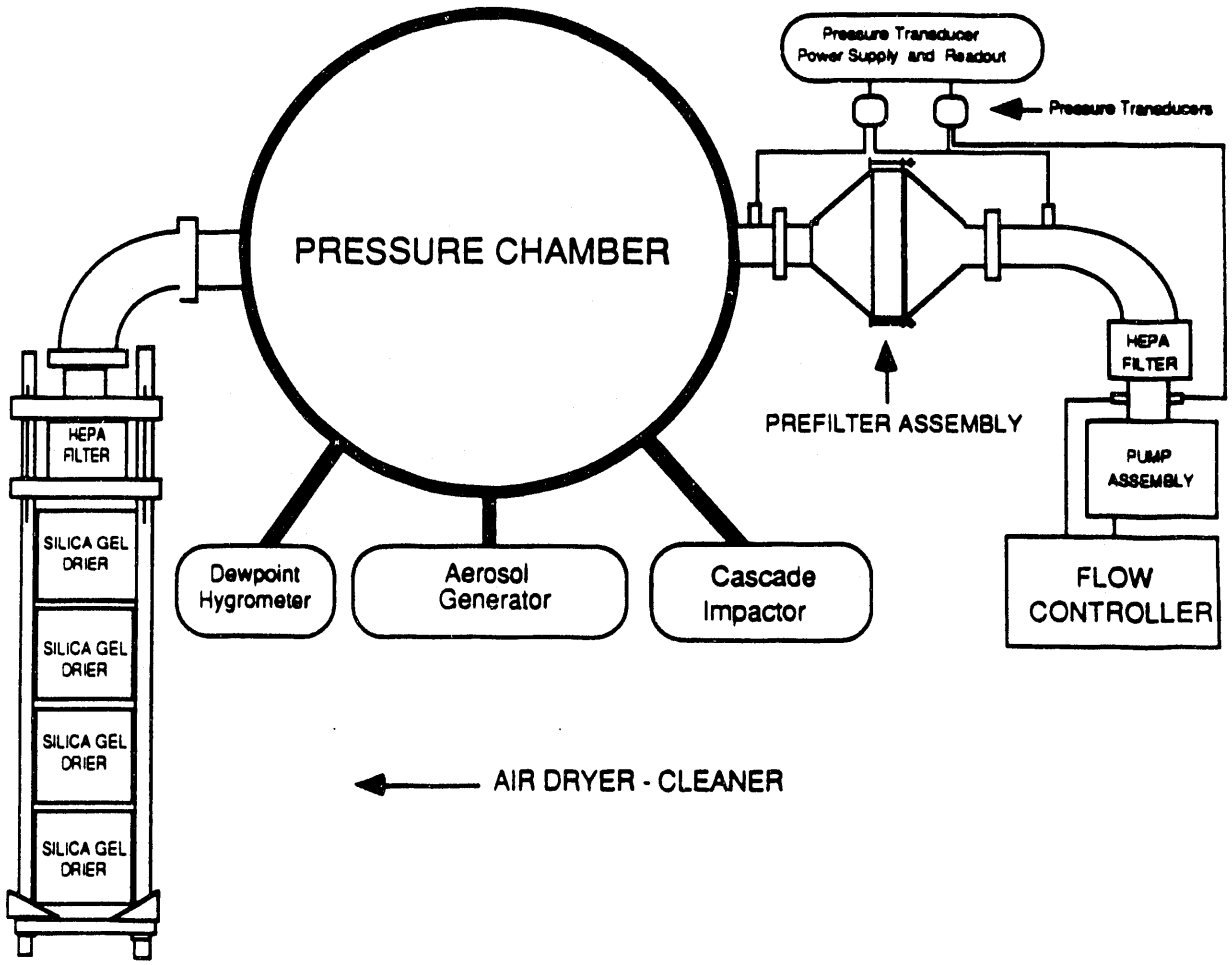

FIGURE 3-1 Experimental apparatus for mass loading tests for both solid and liquid particles.

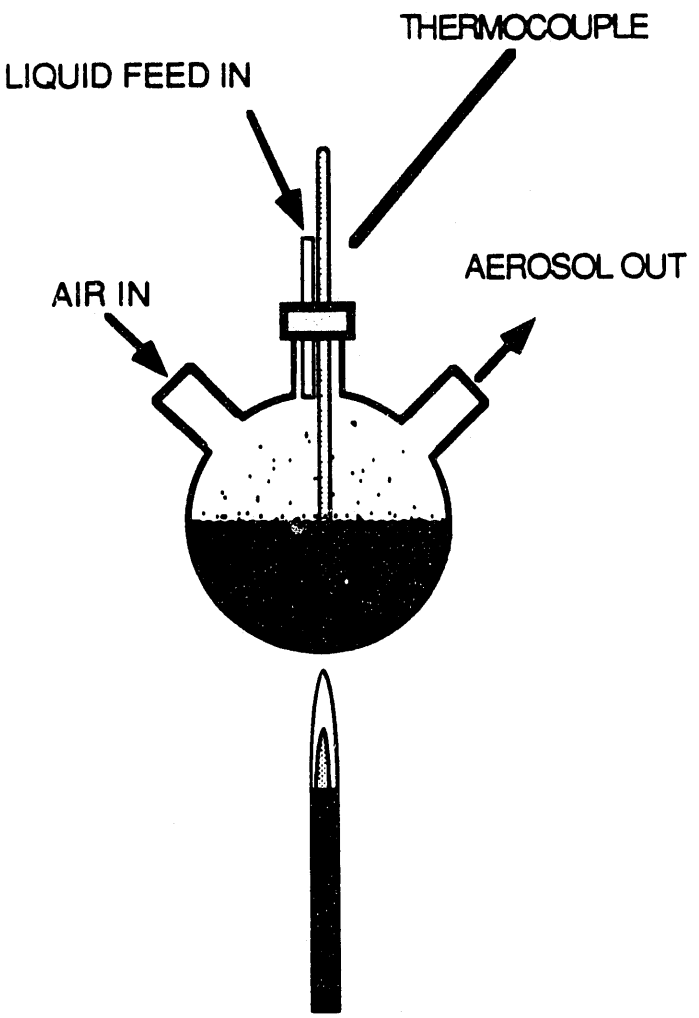

FIGURE 3-2 Diagram of the evaporation-condensation aerosol generator.

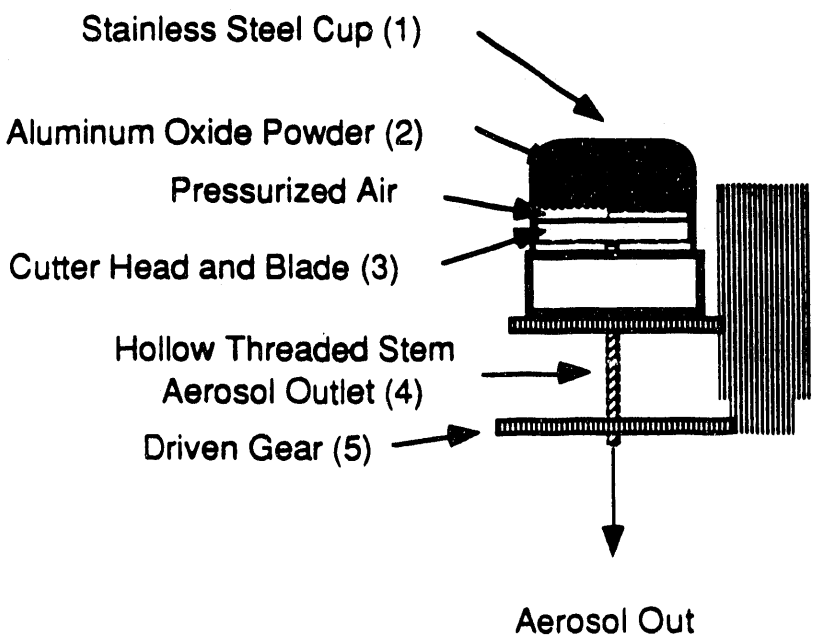

FIGURE 3-3. Diagram of BGI Wright dust feeder.

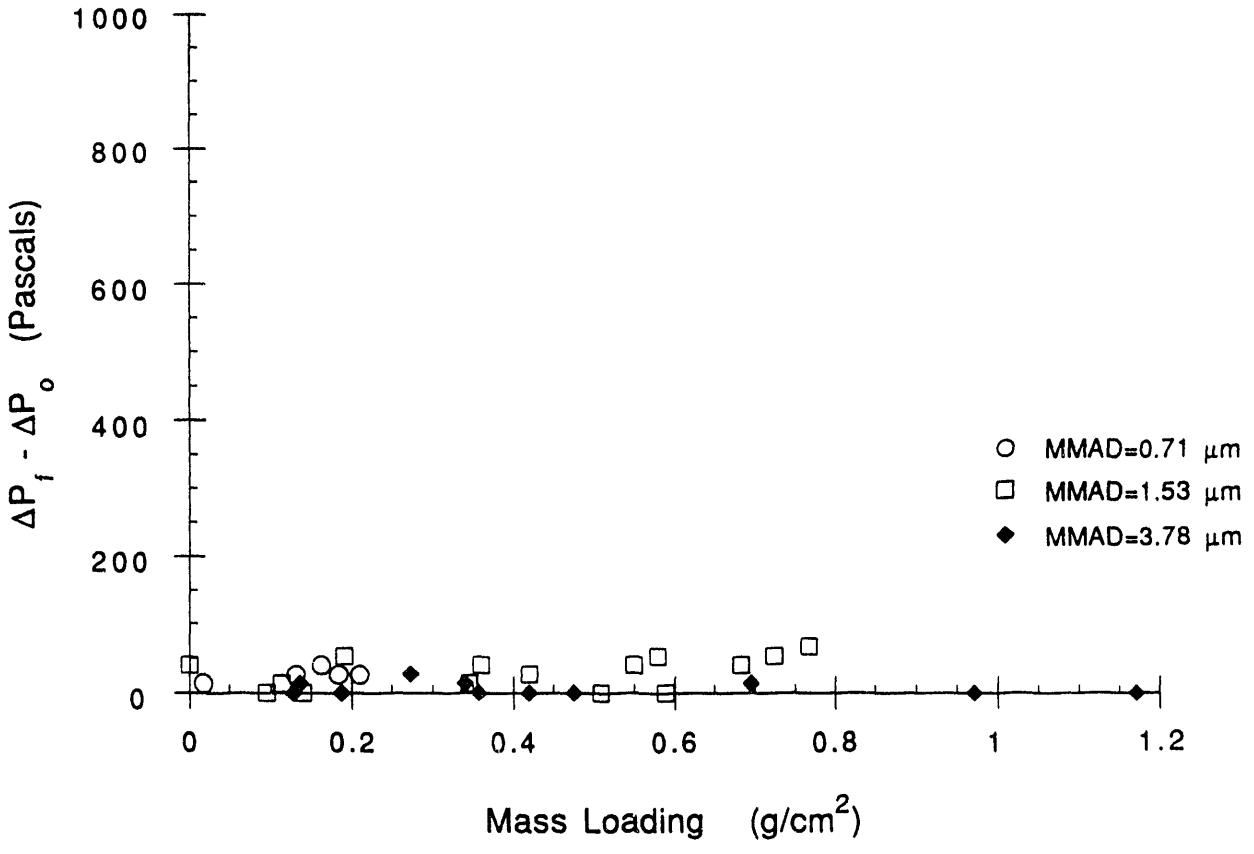

FIGURE 3-4 Mass loading -vs- net pressure change for liquid particles on SRS prefilter material at a face velocity of 152 cm/s. Three particle sizes were studied, each MMAD being the average of tests done for that specific size. Two liquid solutions were used, di-ethylene glycol and dioctyl phthalate.

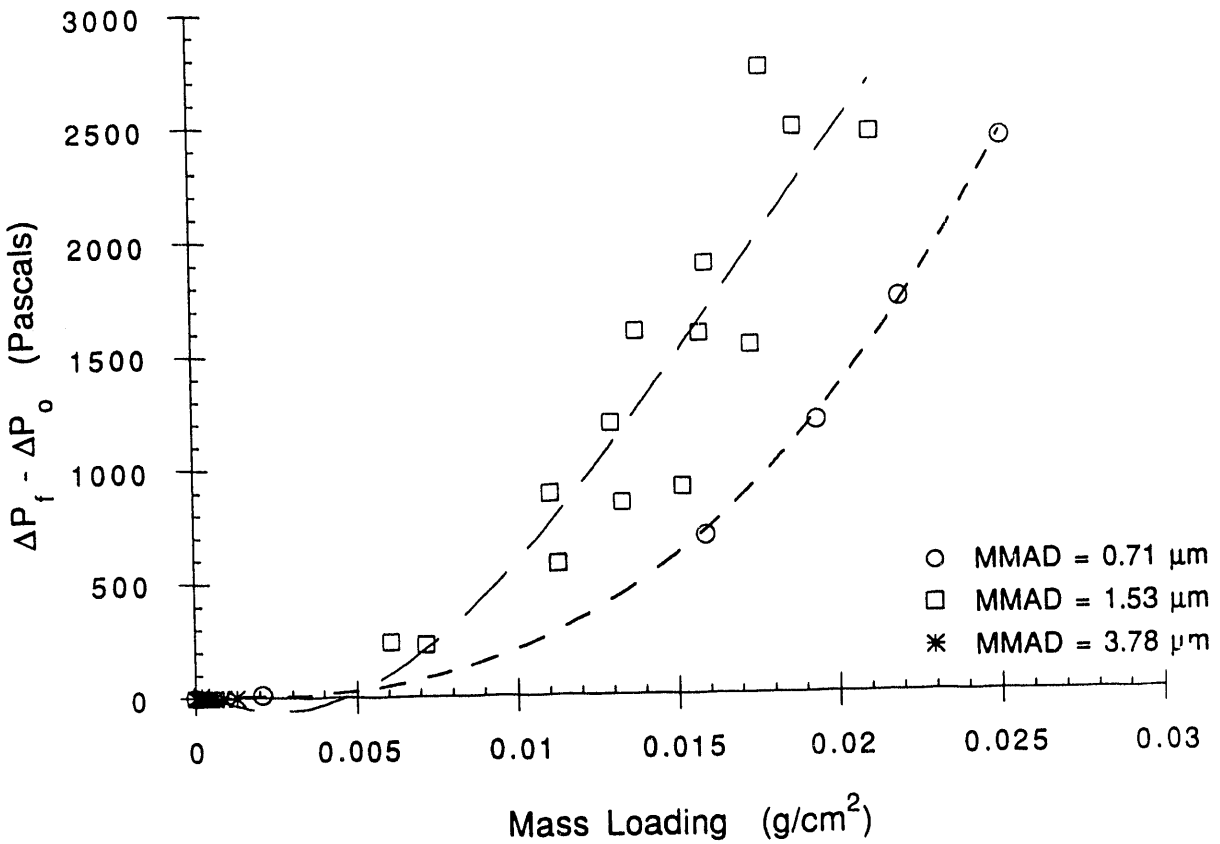

FIGURE 3-5 Mass loading -vs- net pressure change for liquid particles on SRS HEPA filter media at a face velocity of 3 cm/s. Three particle sizes were studied, each MMAD being the average of tests done for that specific size. Two liquid solutions were used, di-ethylene glycol and dioctyl phthalate.

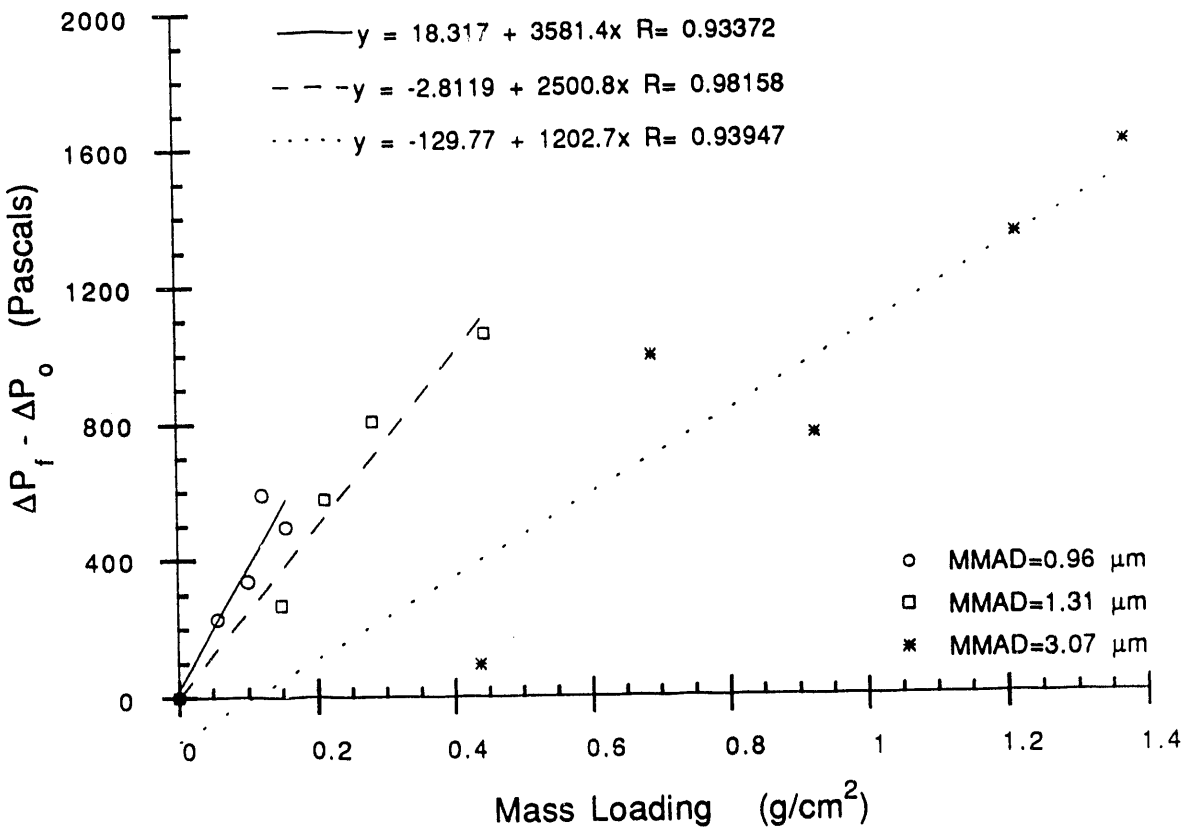

FIGURE 3-6 Mass loading -vs- the net pressure change for solid particles on SRS prefilter material at a face velocity of 152 cm/s. Three particle sizes were studied, each MMAD being the average of tests done for that specific size, using aluminum oxide powder.

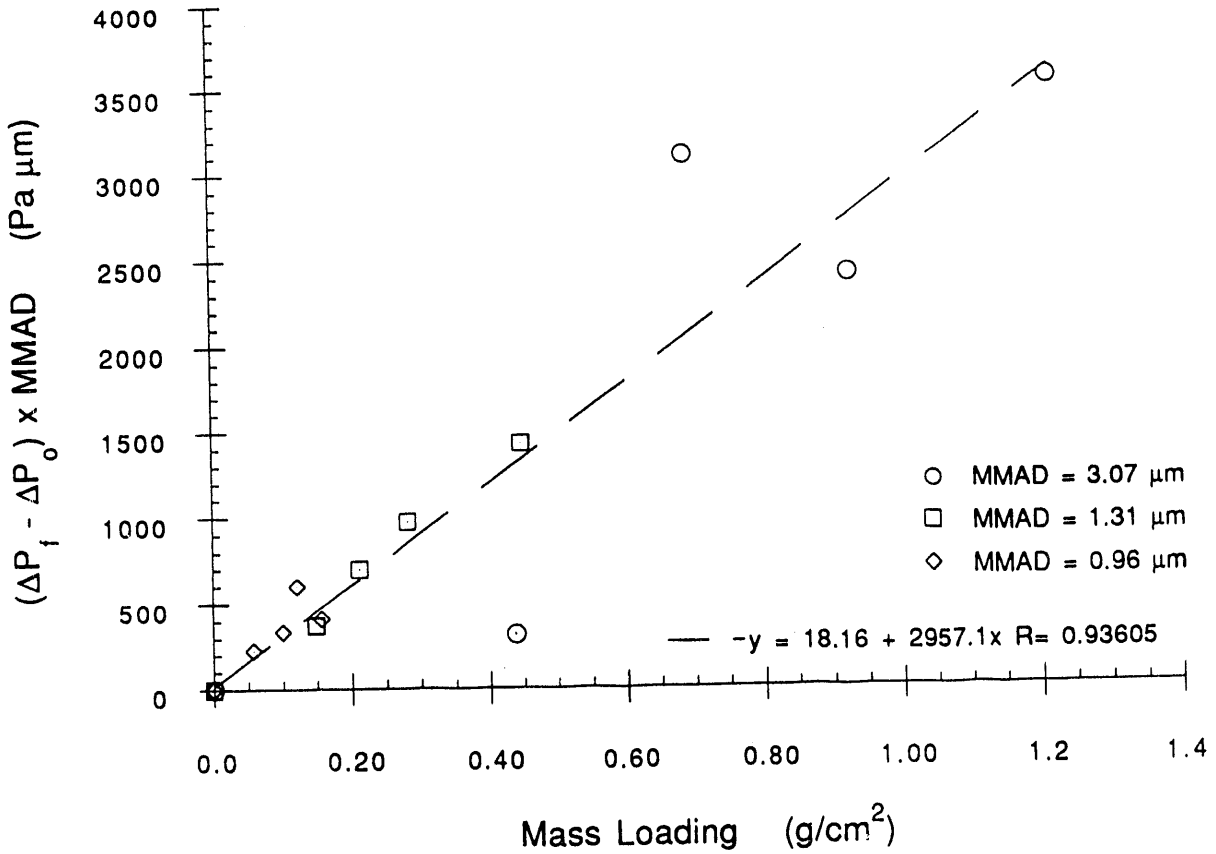

FIGURE 3-7 Mass loading -vs- the product of net pressure change and MMAD for solid particles on SRS prefilter material at a face velocity of 152 cm/s. Three particle sizes were studied, each MMAD being the average of tests done for that specific size, using aluminum oxide powder.

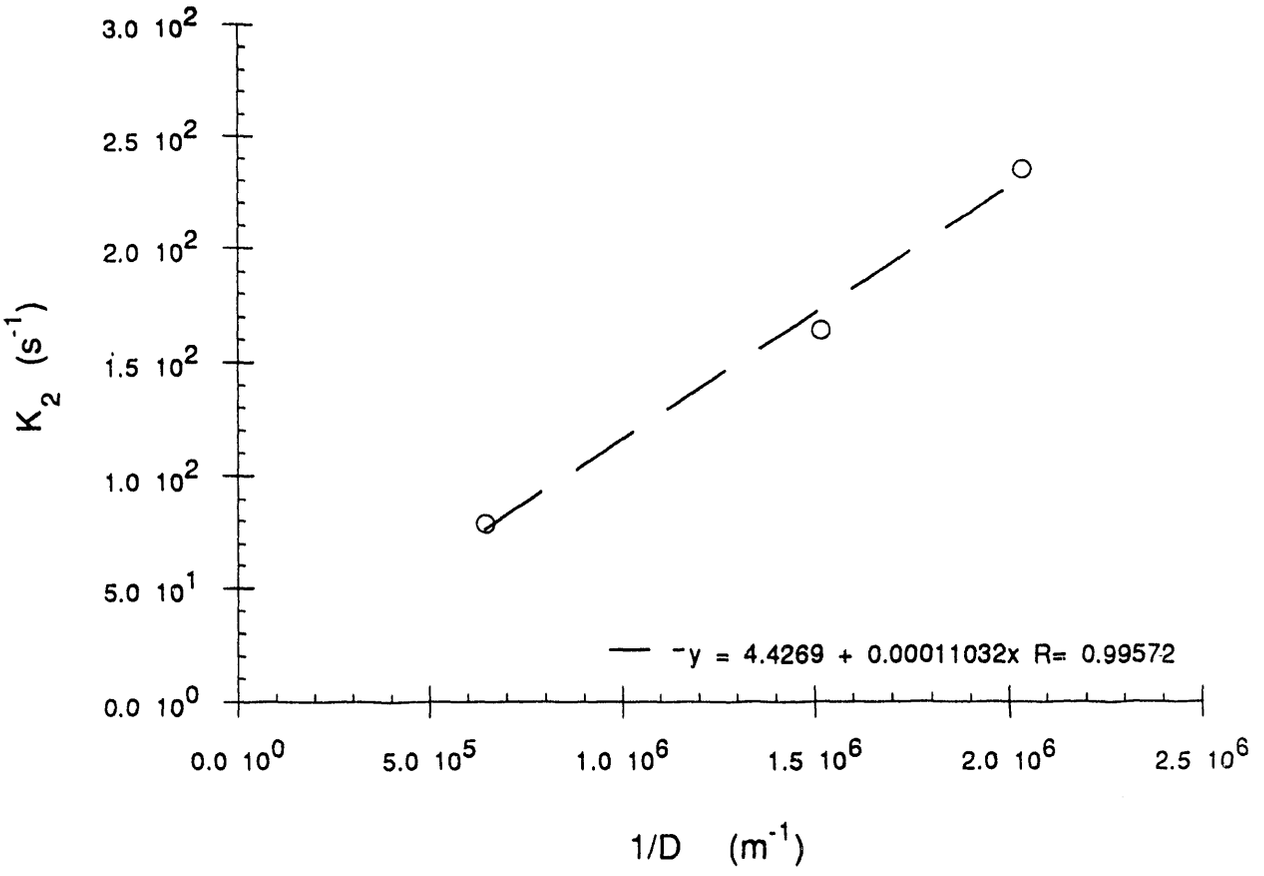

FIGURE 3-8 The specific resistance of aluminum oxide filter cakes for SRS prefilter material plotted as a function of the inverse of the MMAD.

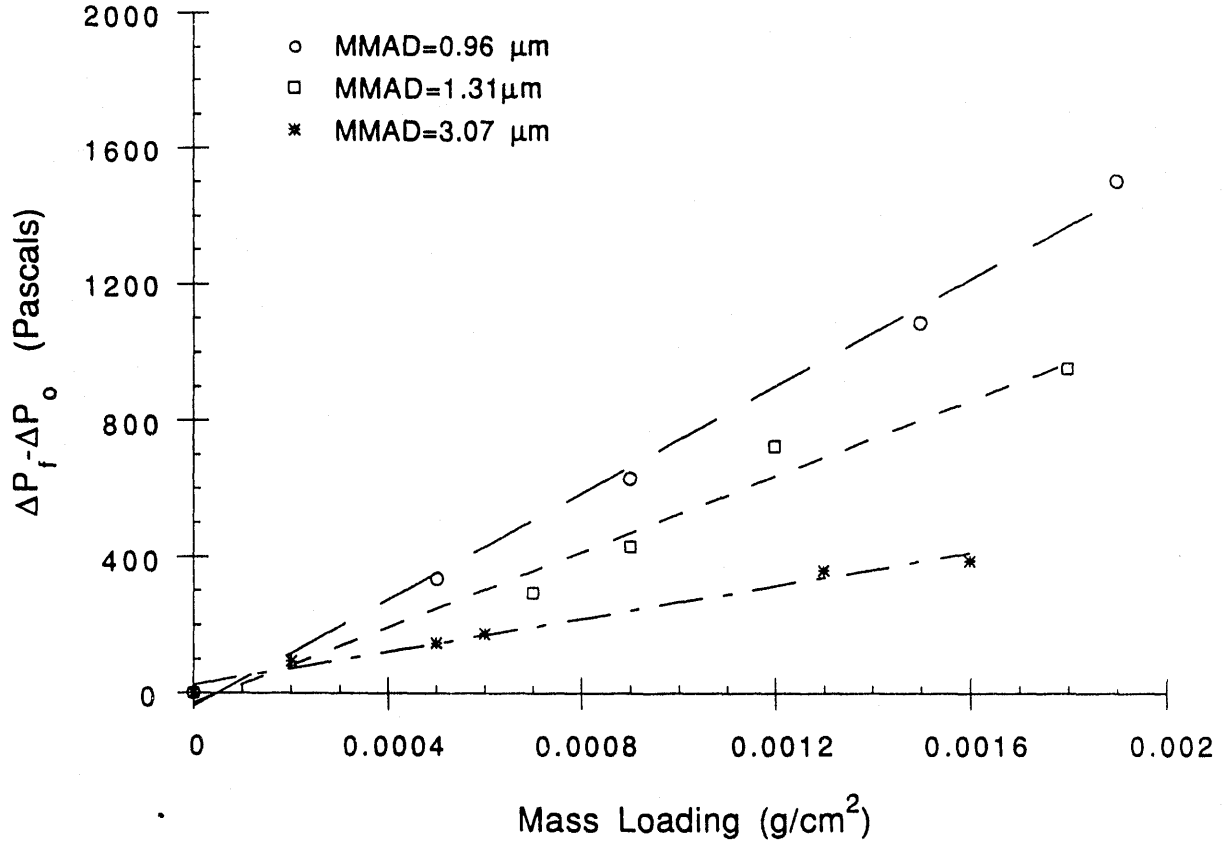

FIGURE 3-9 Mass loading -vs- net pressure change for solid particles on SRS HEPA filter media at a face velocity of 3 cm/s. Three particle sizes of aluminum oxide powder were studied, each MMAD being the average of tests done for that specific size.

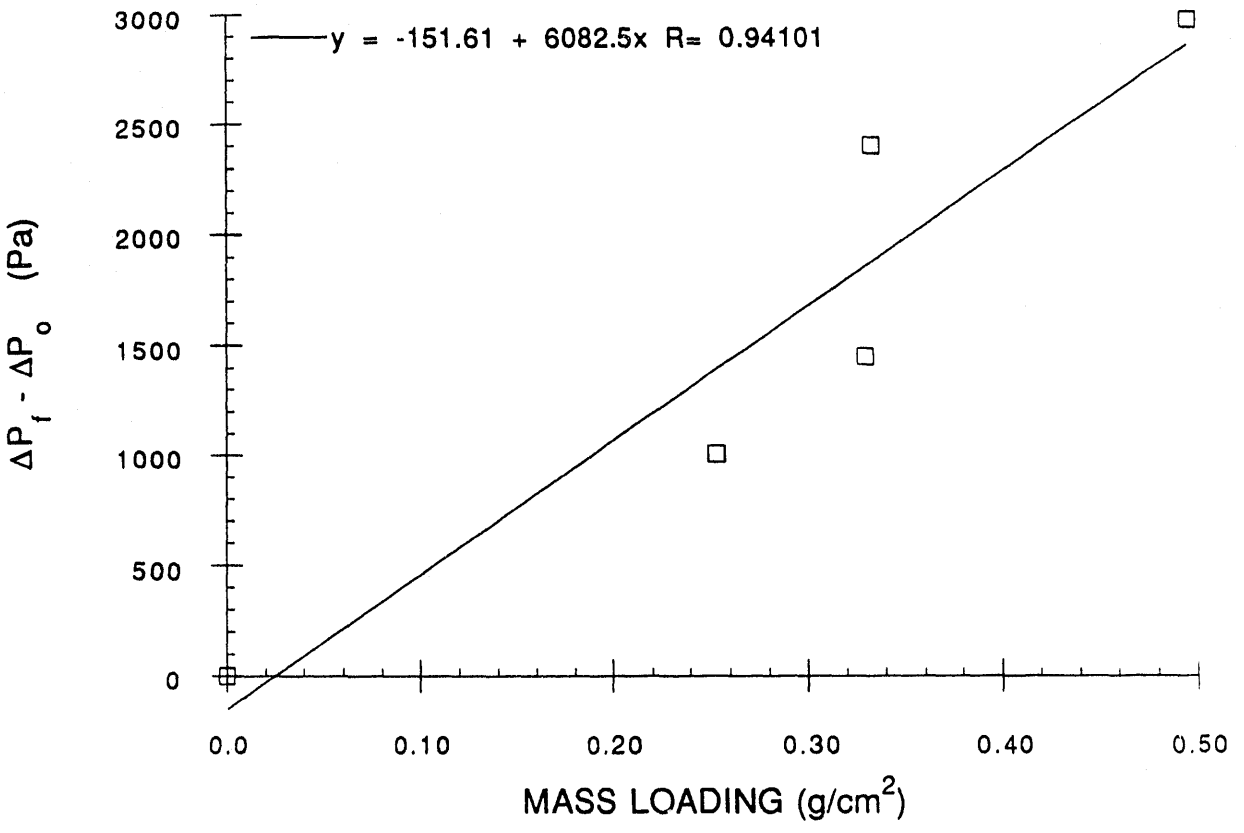

FIGURE 3-10 Mass loading -vs- net pressure change for a combined solid and liquid aerosol on the SRS prefilter material at a face velocity of 152 cm/s. The average MMAD is 2.5 μm for particles consisting of aluminum oxide powder and di-ethylene glycol.

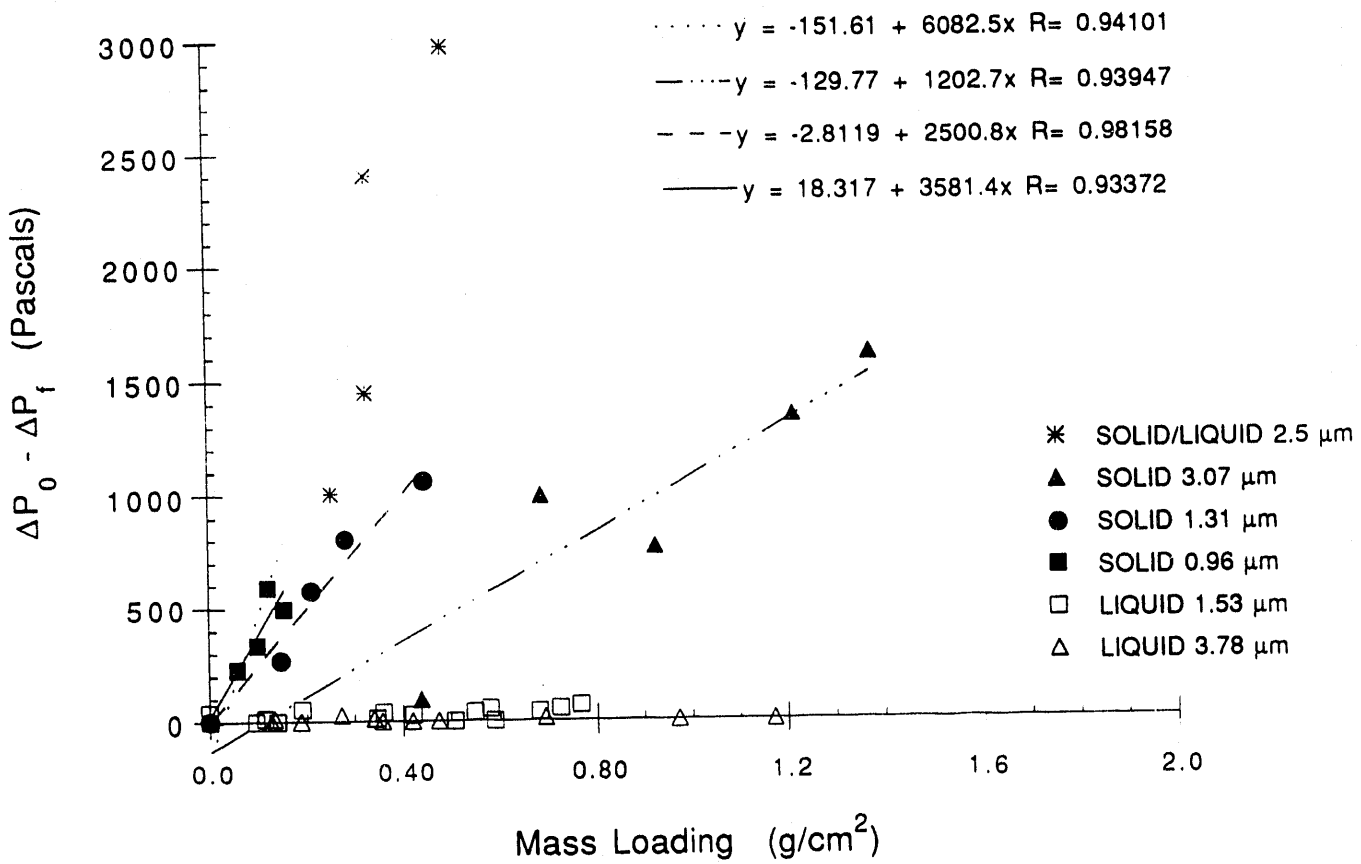

FIGURE 3-11 Mass loading -vs- net pressure change for solid, liquid and mixed solid/liquid particles on SRS prefilter material at a face velocity of 152 cm/s.

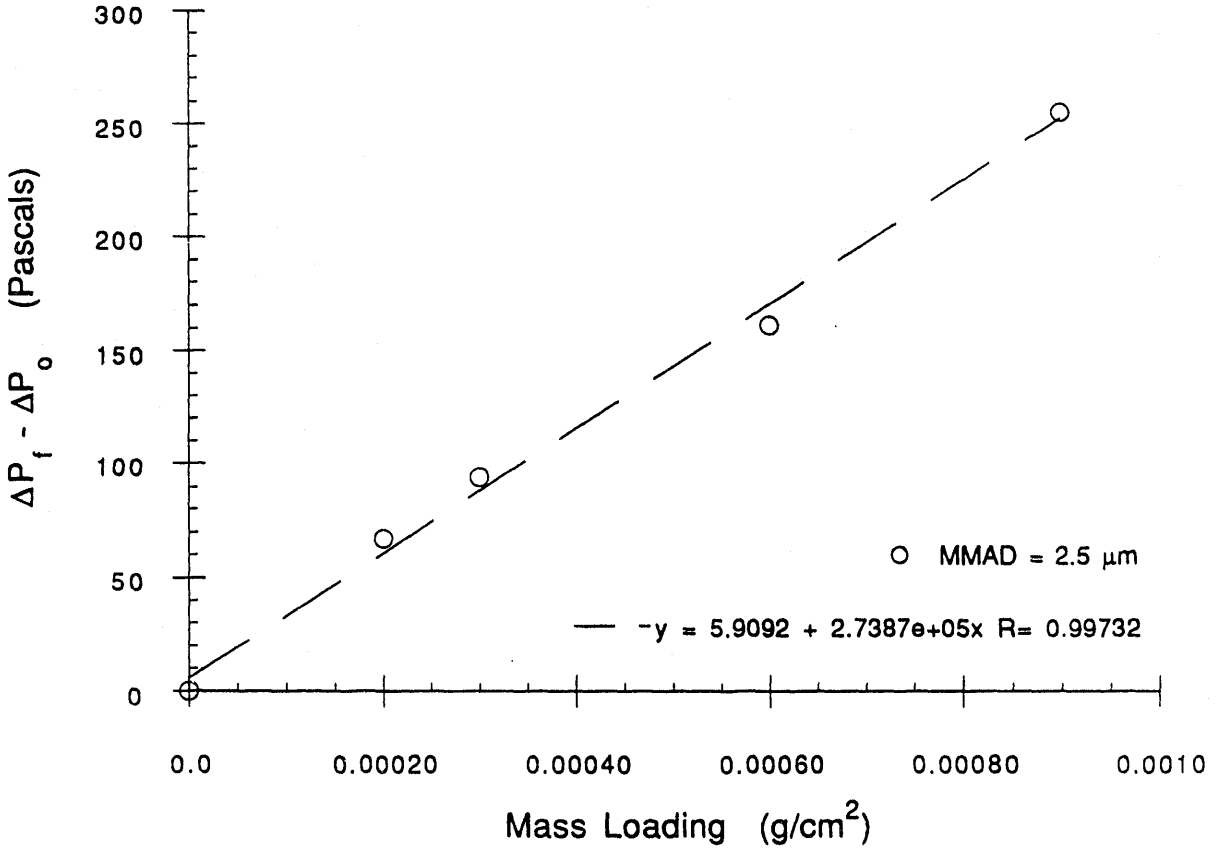

FIGURE 3-12 Mass loading -vs- net pressure change for a combined solid and liquid aerosol on the SRS HEPA filter media at a face velocity of 3 cm/s. The average MMAD is 2.5 µm for particles consisting of aluminum oxide powder and di-ethylene glycol.

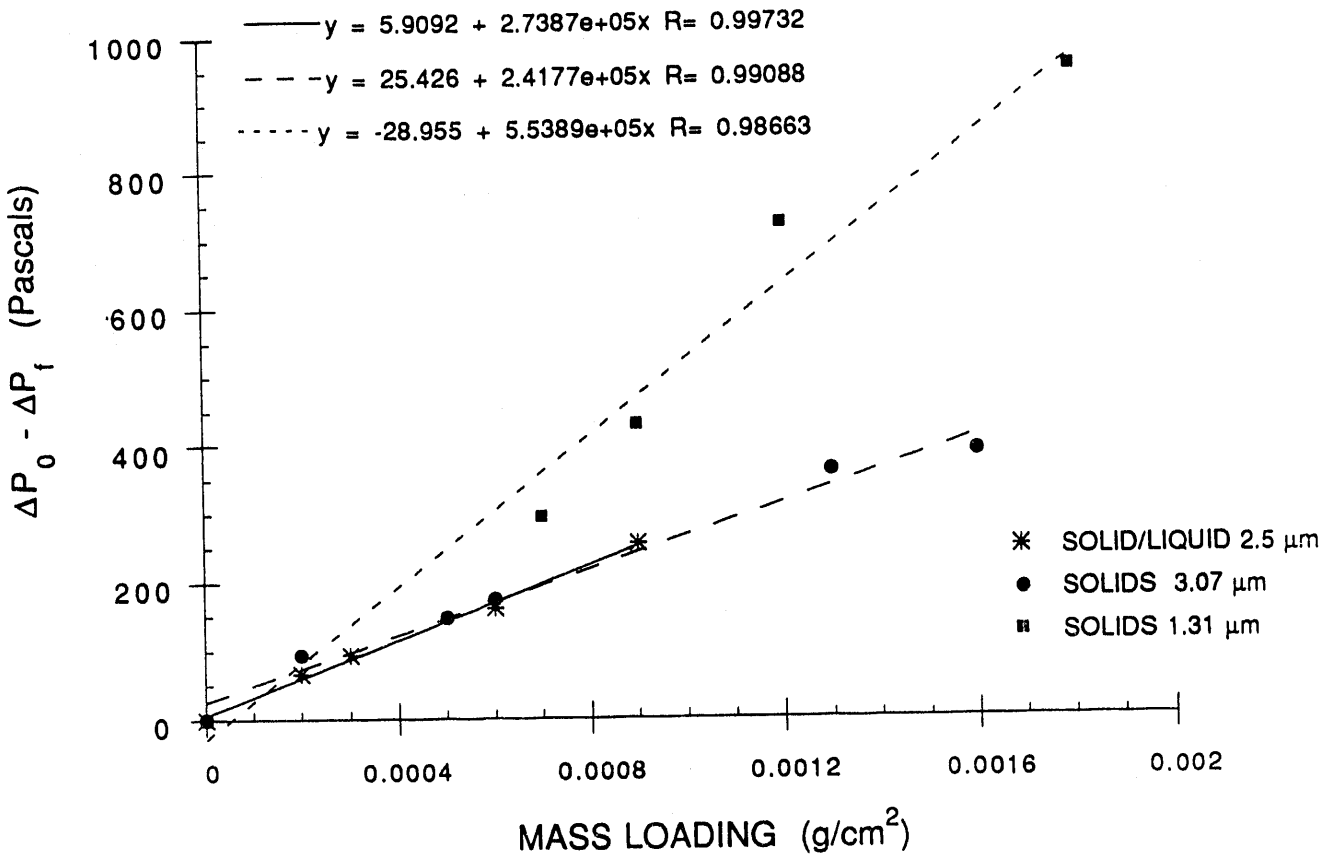

FIGURE 3-13 Mass loading -vs- net pressure change for solid and mixed solid/liquid particles on SRS HEPA filter media at a face velocity of 3 cm/s.

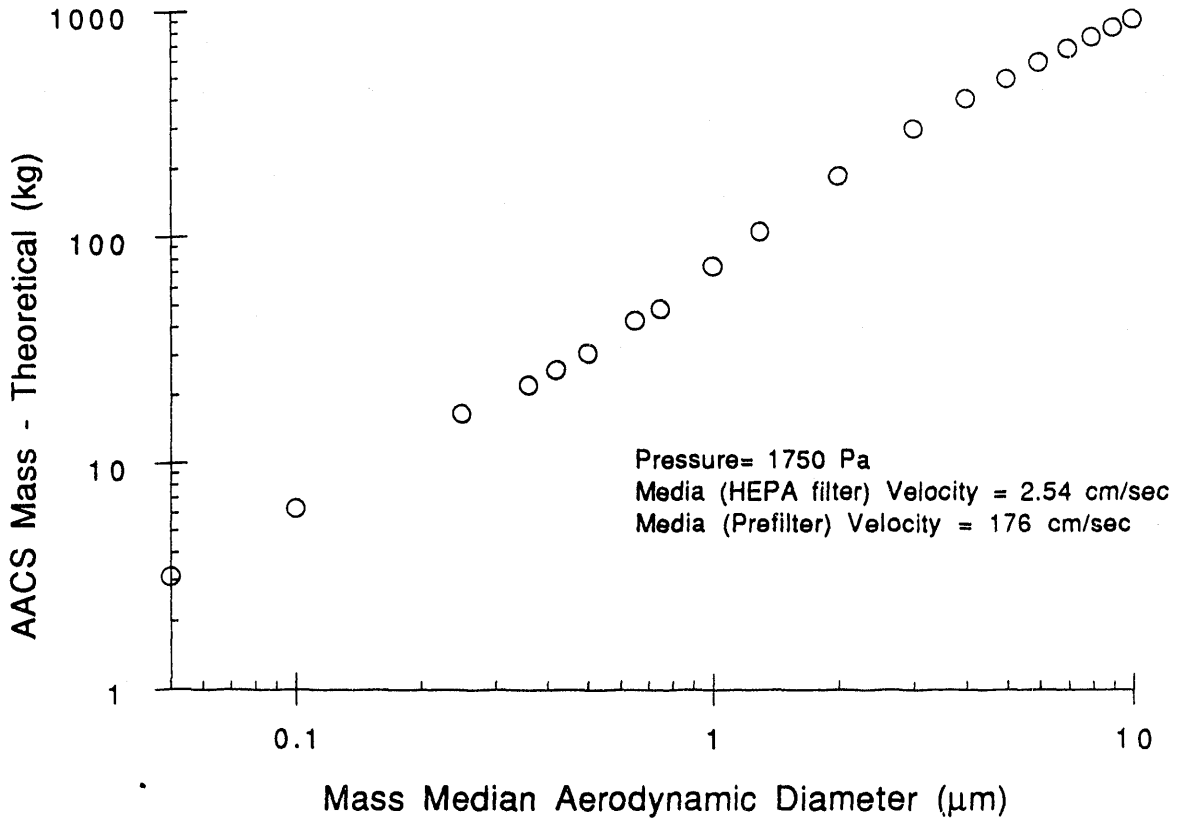

FIGURE 4-1 Predicted AACS mass loading as a function of particle size on the AACS based on experimental data from efficiency and mass loading tests at a pressure of 1750 Pa. Challenge aerosol consisted of solid particles at a velocity through the prefilter of 176 cm/s and through the HEPA filter of 2.54 cm/s.

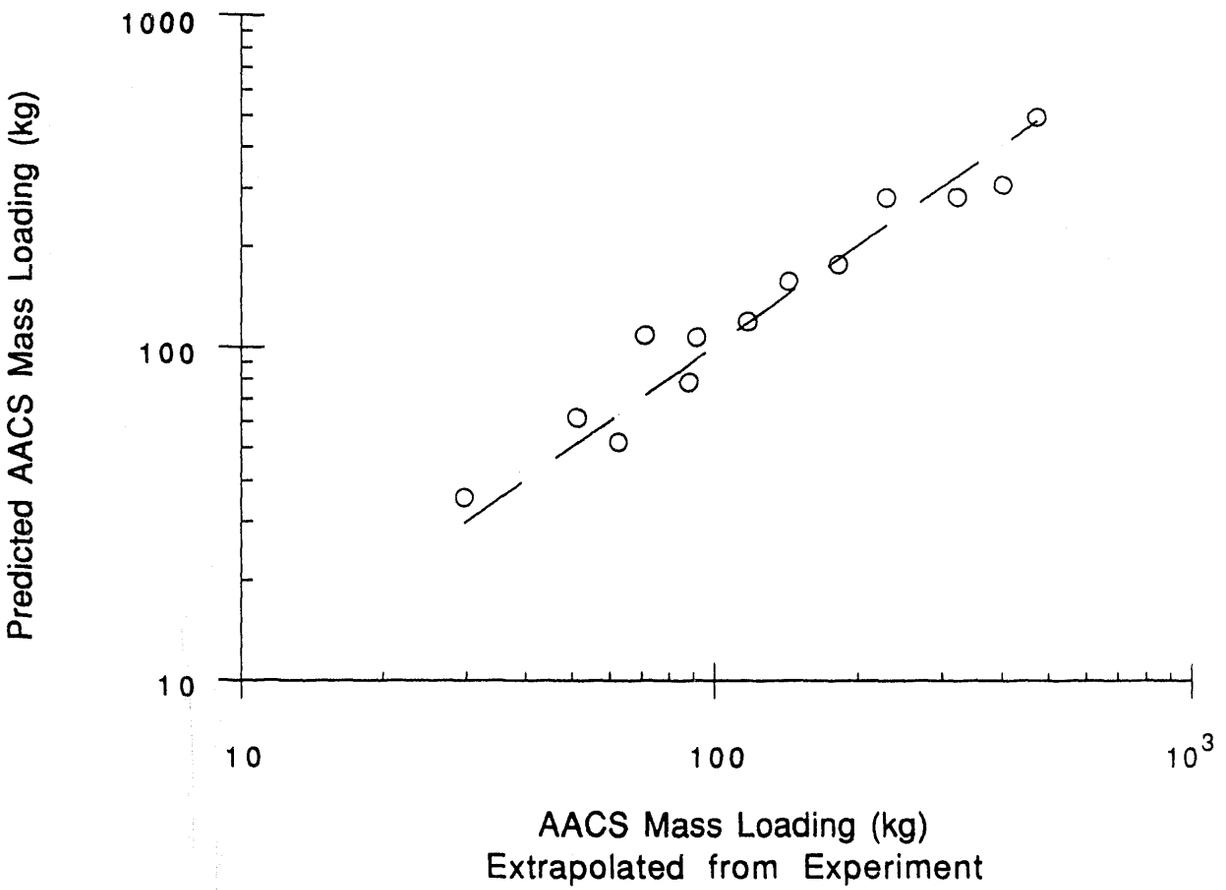

Figure 4-2 Comparison between the predicted AACS mass loading based on calculations involving empirical relations for the efficiency and specific resistance, and extrapolations based on scaling the experimental data to the effective filtration area of the AACS prefilters and HEPA filters.

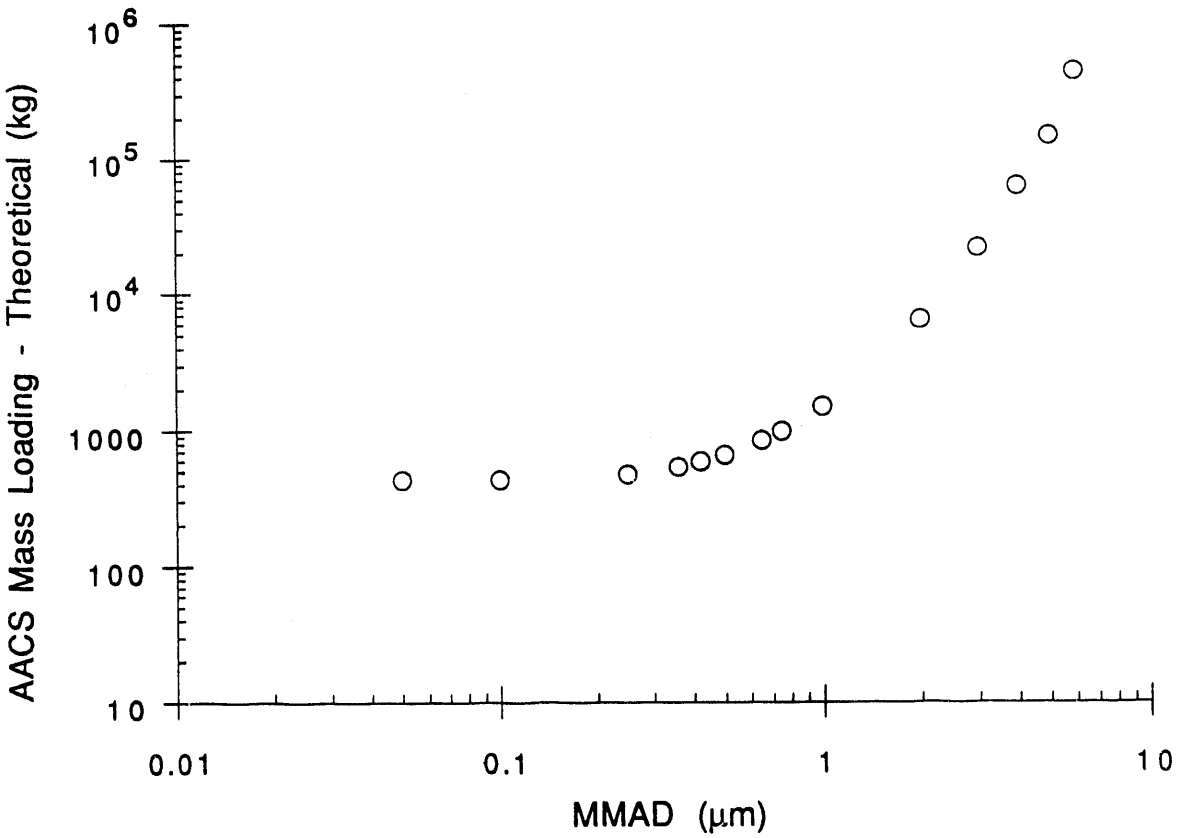

FIGURE 4-3 Predicted AACS mass loading as a function of particle size on the AACS based on experimental data from efficiency and mass loading tests at a pressure of 1750 Pa. Challenge aerosol consisted of liquid particles at a velocity through the prefilter of 152 cm/s and through the HEPA filter of 3 cm/s.

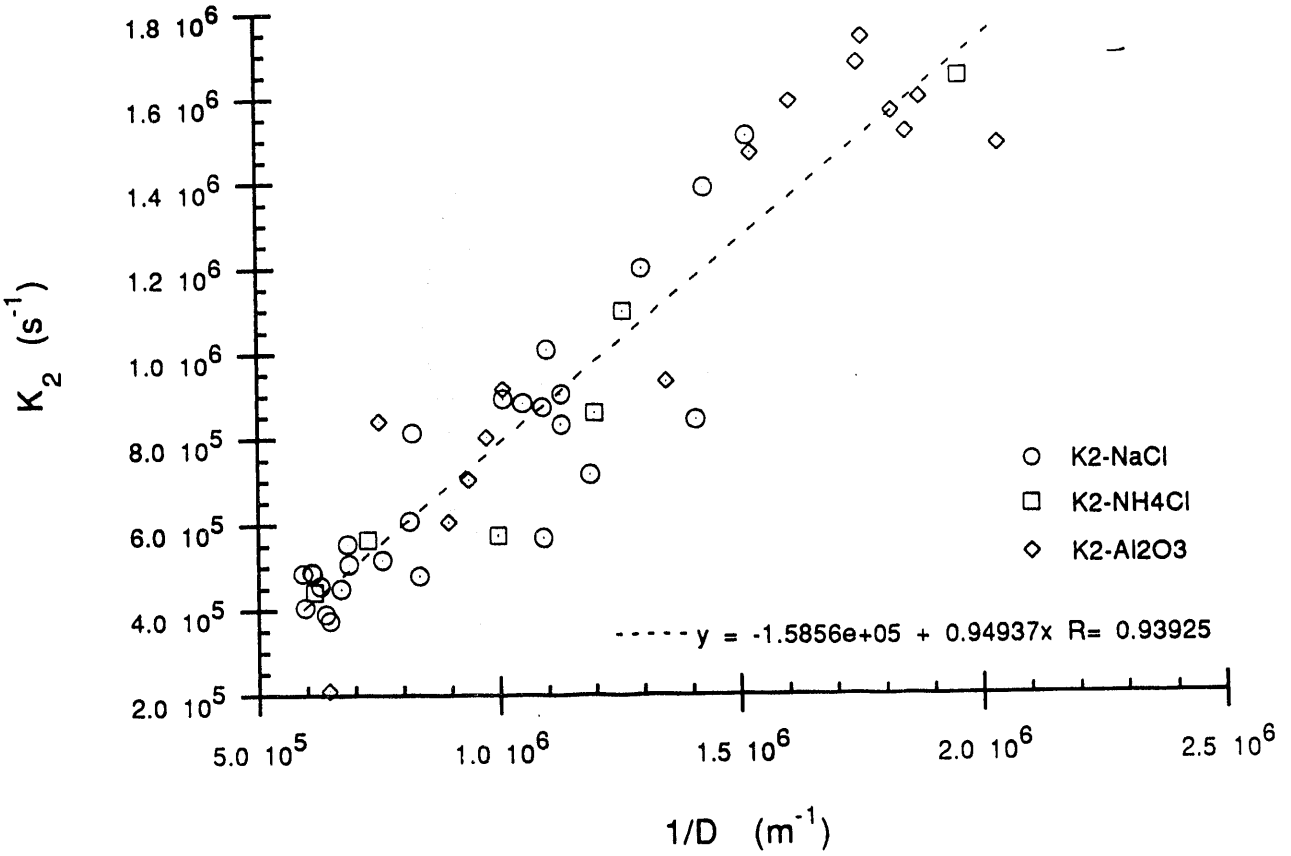

FIGURE B-1 The specific resistance of sodium chloride, ammonium chloride and aluminum oxide filter cakes plotted as a function of the inverse of the MMD on SRS HEPA filter media.

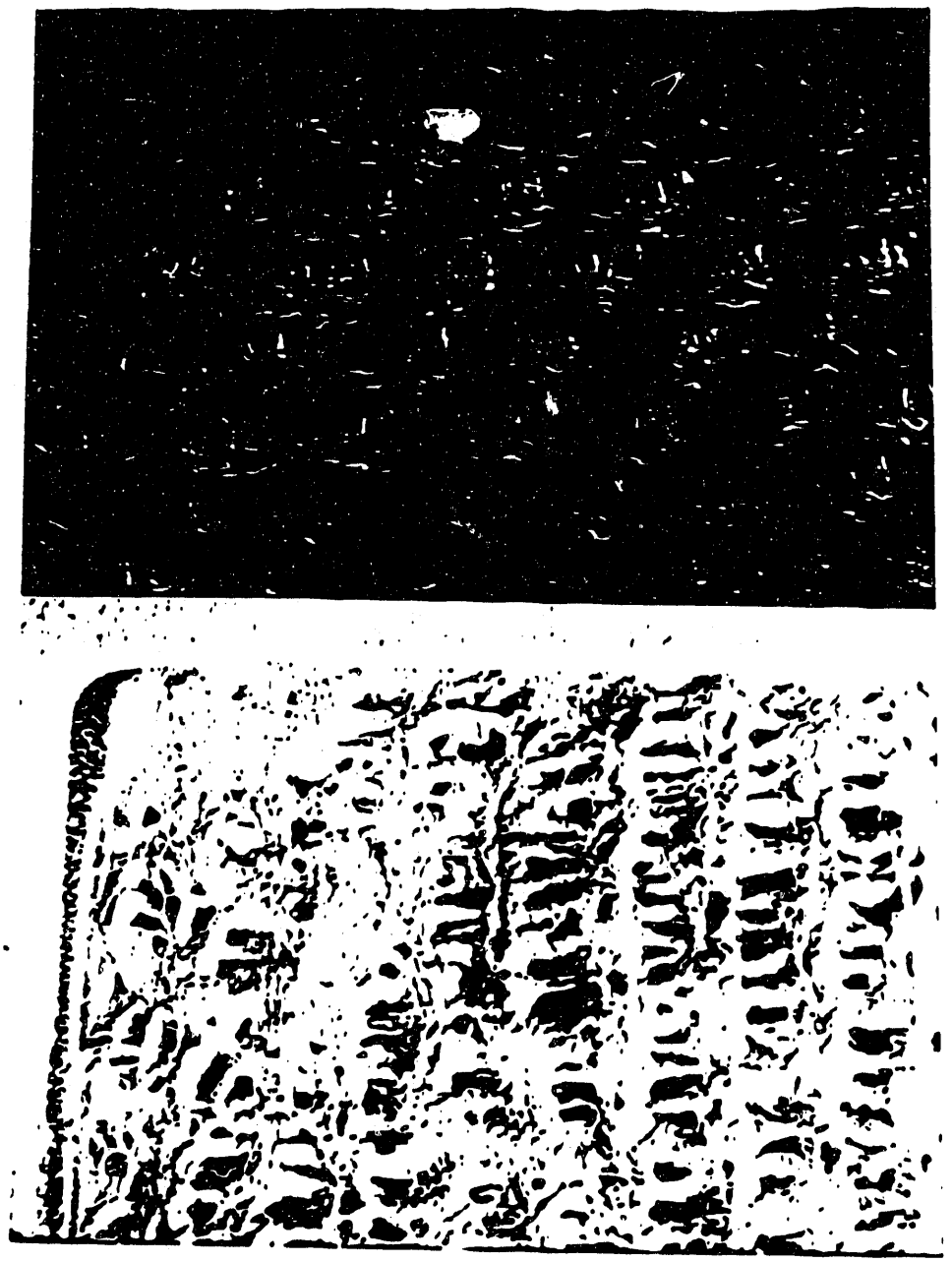

PHOTO 1 Clean SRS prefilter material (top); Upstream view of prefilter material coated with aluminum oxide powder (bottom).

END

DATE
FILMED
3/26/93